

Cite this: *Dalton Trans.*, 2015, **44**, 7292

Phosphine, isocyanide, and alkyne reactivity at pentanuclear molybdenum/tungsten–iridium clusters†

Peter V. Simpson, Michael D. Randles, Vivek Gupta, Junhong Fu, Graeme J. Moxey, Torsten Schwich, Mahbod Morshedi, Marie P. Cifuentes and Mark G. Humphrey*

The trigonal bipyramidal clusters $M_2Ir_3(\mu-CO)_3(CO)_6(\eta^5-C_5H_5)_2(\eta^5-C_5Me_4R)$ ($M = Mo$, $R = Me$ **1a**, $R = H$; $M = W$, $R = Me$, H) reacted with isocyanides to give ligand substitution products $M_2Ir_3(\mu-CO)_3(CO)_5(CNR')(\eta^5-C_5H_5)_2(\eta^5-C_5Me_4R)$ ($M = Mo$, $R = Me$, $R' = C_6H_3Me_2-2,6$ **3a**; $M = Mo$, $R = Me$, $R' = tBu$ **3b**), in which core geometry and metal atom locations are maintained, whereas reactions with PPh_3 afforded $M_2Ir_3(\mu-CO)_4(CO)_4(PPh_3)(\eta^5-C_5H_5)_2(\eta^5-C_5Me_4R)$ ($M = Mo$, $R = Me$ **4a**, **H 4c**; $M = W$, $R = Me$ **4b**, H), with retention of core geometry but with effective site-exchange of the precursors' apical Mo/W with an equatorial Ir. Similar treatment of trigonal bipyramidal $MIr_4(\mu-CO)_3(CO)_7(\eta^5-C_5H_5)(\eta^5-C_5Me_5)$ ($M = Mo$ **2a**, W **2b**) with PPh_3 afforded the mono-substitution products $MIr_4(\mu-CO)_3(CO)_6(PPh_3)(\eta^5-C_5H_5)(\eta^5-C_5Me_5)$ ($M = Mo$ **5a**; $M = W$ **5b**), and further reaction of the molybdenum example **5a** with excess PPh_3 afforded the bis-substituted cluster $MoIr_4(\mu_3-CO)_2(\mu-CO)_2(CO)_4(PPh_3)_2(\eta^5-C_5H_5)(\eta^5-C_5Me_5)$ (**6**). Reaction of **1a** with diphenylacetylene proceeded with alkyne coordination and $C\equiv C$ cleavage, affording $Mo_2Ir_3(\mu_4-\eta^2-PhC_2Ph)(\mu_3-CPh)_2(CO)_4(\eta^5-C_5H_5)_2(\eta^5-C_5Me_5)$ (**7a**) together with an isomer. Reactions of **2a** and **2b** with $PhC\equiv CR$ afforded $MIr_4(\mu_3-\eta^2-PhC_2R)(\mu_3-CO)_2(CO)_6(\eta^5-C_5H_5)(\eta^5-C_5Me_5)$ ($M = Mo$, $R = Ph$ **8a**; $M = W$, $R = Ph$ **8b**, H ; $M = W$, $R = C_6H_4(C_2Ph)-3$ **9a**, $C_6H_4(C_2Ph)-4$), while addition of 0.5 equivalents of the diynes 1,3- $C_6H_4(C_2Ph)_2$ and 1,4- $C_6H_4(C_2Ph)_2$ to $WIr_4(\mu-CO)_3(CO)_7(\eta^5-C_5H_5)(\eta^5-C_5Me_5)$ gave the linked clusters $[WIr_4(CO)_8(\eta^5-C_5H_5)(\eta^5-C_5Me_5)]_2(\mu_6-\eta^4-PhC_2C_6H_4(C_2Ph)-X)$ ($X = 3, 4$). The structures of **3a**, **4a–4c**, **5b**, **6**, **7a**, **8a**, **8b** and **9a** were determined by single-crystal X-ray diffraction studies, establishing the core isomerization of **4**, the site selectivity for ligand substitution in **3–6**, the alkyne $C\equiv C$ dismutation in **7**, and the site of alkyne coordination in **7–9**. For clusters **3–6**, ease of oxidation increases on increasing donor strength of ligand, increasing extent of ligand substitution, replacing Mo by W, and decreasing core Ir content, the Ir-rich clusters **5** and **6** being the most reversible. For clusters **7–9**, ease of oxidation diminishes on replacing Mo by W, increasing the Ir content, and proceeding from mono-yne to diyne, although the latter two changes are small. *In situ* UV-vis-near-IR spectroelectrochemical studies of the (electrochemically reversible) reduction process of **8b** were undertaken, the spectra becoming increasingly broad and featureless following reduction. The incorporation of isocyanides, phosphines, or alkyne residues in these pentanuclear clusters all result in an increased ease of oxidation and decreased ease of reduction, and thereby tune the electron richness of the clusters.

Received 5th February 2015,

Accepted 11th March 2015

DOI: 10.1039/c5dt00525f

www.rsc.org/dalton

Research School of Chemistry, Australian National University, Canberra, ACT 2601, Australia. E-mail: Mark.Humphrey@anu.edu.au; Fax: +61 2 6125 0750;

Tel: +61 2 6125 2927

† Electronic supplementary information (ESI) available: Synthesis and spectroscopic characterization details for **3b**, **4b**, **4c**, **4d**, **5b**, **8b**, **8c**, **9b**, and **10b**, X-ray crystallographic data in CIF format for **3a**, **4a–4c**, **5b**, **6**, **7a**, **8a**, **8b**, and **9a**, crystal data for **3a**, **4a–4c**, **5b**, **6**, **7a**, **8a**, **8b**, and **9a**, ORTEP plots of **4b**, **4c**, **8a**, and **8b**, and one of the two crystallographically distinct molecules of each of **6** and **7a**, and UV-vis spectral data during reduction of **8b**. CCDC 1018833 (**3a**), 1018834 (**4a**), 1018835 (**4b**), 1018836 (**4c**), 1018837 (**5b**), 1018838 (**6**), 1018839 (**7a**), 1018840 (**8a**), 1018841 (**8b**), and 1018842 (**9a**). For ESI and crystallographic data in CIF or other electronic format see DOI: 10.1039/c5dt00525f

Introduction

Transition metal carbonyl clusters have attracted long-standing interest.¹ Due to ease of synthetic access to such species, considerable effort has been expended defining the reactivity of low-nuclearity (M_n , $n = 3, 4$) homometallic clusters; medium- ($n = 5, 6$) and higher-nuclearity ($n \geq 7$) examples are comparatively less-explored, although the increasing metal loading on an organic substrate that is possible with such clusters may afford enhanced or heretofore unobserved forms of activation.² In this context, heterometallic clusters are also less explored,

with the vast majority of examples studied thus far incorporating metal atoms from either the same transition series group or from adjacent groups; mixed-metal clusters containing disparate metals are still under-represented, despite the fact that the resultant (more) polar metal–metal bonds may provide additional avenues for substrate activation.³ The varying constituent metals of the cluster core in mixed-metal clusters also afford the possibility of probing metallo-, bond-, and site-selectivity for a variety of reagents. Reactivity studies of medium- and high-nuclearity mixed-metal clusters incorporating disparate metals are therefore of considerable interest.

Phosphines and alkynes are arguably the archetypal substrates for exploring two-electron donor ligand and cluster-bound *C*-ligand chemistry, respectively, while isocyanides CNR are carbonyl-like ligands with considerable flexibility in composition. We have previously reported extensive studies of the phosphine, isocyanide, and alkyne chemistry of the tetrahedral group 6–group 9 transition metal clusters $M\text{Ir}_3(\text{CO})_{11}(\eta^5\text{-C}_5\text{R}_5)$ and $M_2\text{Ir}_2(\text{CO})_{10}(\eta^5\text{-C}_5\text{R}_5)_2$ ($M = \text{Mo}, \text{W}$; $\text{R}_5 = \text{H}_5, \text{H}_4\text{Me}, \text{HMe}_4, \text{Me}_5$),⁴ defining the isomers' structures, distribution and CO fluxionality resultant upon mono- to tris-phosphine and isocyanide substitution, and affording an array of unique aryl-diyne- and -triyne-linked oligoclusters. However, as mentioned above, the diversity of the chemistry is constrained by the low-nuclearity of the cluster. We very recently reported the high-yielding syntheses and structural characterization of the trigonal bipyramidal clusters $M_2\text{Ir}_3(\mu\text{-CO})_3(\text{CO})_6(\eta^5\text{-C}_5\text{H}_5)_2(\eta^5\text{-C}_5\text{Me}_4\text{R})$ ($\text{R} = \text{Me}, \text{M} = \text{Mo}$ **1a**, **W 1b**; $\text{R} = \text{H}, \text{M} = \text{Mo}$ **1c**, **W 1d**) and $M\text{Ir}_4(\mu\text{-CO})_3(\text{CO})_7(\eta^5\text{-C}_5\text{H}_5)(\eta^5\text{-C}_5\text{Me}_4\text{R})$ ($\text{R} = \text{Me}, \text{M} = \text{Mo}$ **2a**, **W 2b**; $\text{R} = \text{H}, \text{M} = \text{Mo}$ **2c**, **W 2d**).⁵ We report herein the results of studies exploring the isocyanide and phosphine substitution chemistry of these pentanuclear clusters, as well as their reactivity towards arylalkynes, with the products from these studies featuring cluster core isomerization, site selectivity for ligand substitution, and alkyne $\text{C}\equiv\text{C}$ dismutation.

Experimental

General conditions and reagents

Reactions were performed under an atmosphere of nitrogen using standard Schlenk techniques, although no special precautions were taken to exclude air in the work-ups. Reactions were monitored regularly by IR spectroscopy to ensure consumption of the starting cluster. Solvents used in reactions were AR grade and distilled under nitrogen using standard methods: CH_2Cl_2 over CaH_2 , toluene and THF over sodium benzophenone ketyl. All other solvents and other reagents were obtained commercially and were used as received. Petrol refers to a fraction of boiling range 60–80 °C. Cluster products were purified by preparative thin-layer chromatography (TLC) on 20×20 cm glass plates coated with Merck GF₂₅₄ silica gel (0.5 mm). Analytical TLC was conducted on aluminium sheets coated with 0.25 mm Merck GF₂₅₄ silica gel. Literature procedures were used to synthesize **1a–1d** and **2a–2d**.⁵ The syntheses of $\text{Mo}_2\text{Ir}_3(\mu\text{-CO})_3(\text{CO})_5(\text{CNC}^t\text{Bu})(\eta^5\text{-C}_5\text{H}_5)_2(\eta^5\text{-C}_5\text{Me}_5)$ (**3b**),

$\text{W}_2\text{Ir}_3(\mu\text{-CO})_4(\text{CO})_4(\text{PPh}_3)(\eta^5\text{-C}_5\text{H}_5)_2(\eta^5\text{-C}_5\text{Me}_5)$ (**4b**), $\text{Mo}_2\text{Ir}_3(\mu\text{-CO})_4(\text{CO})_4(\text{PPh}_3)(\eta^5\text{-C}_5\text{H}_5)_2(\eta^5\text{-C}_5\text{Me}_4\text{H})$ (**4c**), $\text{W}_2\text{Ir}_3(\mu\text{-CO})_4(\text{CO})_4(\text{PPh}_3)(\eta^5\text{-C}_5\text{H}_5)_2(\eta^5\text{-C}_5\text{Me}_4\text{H})$ (**4d**), $\text{WIr}_4(\mu\text{-CO})_3(\text{CO})_6(\text{PPh}_3)(\eta^5\text{-C}_5\text{H}_5)(\eta^5\text{-C}_5\text{Me}_5)$ (**5b**), $\text{WIr}_4(\mu_3\text{-}\eta^2\text{-PhC}_2\text{Ph})(\mu_3\text{-CO})_2(\text{CO})_6(\eta^5\text{-C}_5\text{H}_5)(\eta^5\text{-C}_5\text{Me}_5)$ (**8b**), $\text{WIr}_4(\mu_3\text{-}\eta^2\text{-HC}_2\text{Ph})(\text{CO})_8(\eta^5\text{-C}_5\text{H}_5)(\eta^5\text{-C}_5\text{Me}_5)$ (**8c**), $\text{WIr}_4(\mu_3\text{-}\eta^2\text{-PhCCC}_6\text{H}_4(\text{C}_2\text{Ph})\text{-4})(\text{CO})_8(\eta^5\text{-C}_5\text{H}_5)(\eta^5\text{-C}_5\text{Me}_5)$ (**9b**) and $[\text{WIr}_4(\text{CO})_8(\eta^5\text{-C}_5\text{H}_5)(\eta^5\text{-C}_5\text{Me}_5)]_2(\mu_6\text{-}\eta^4\text{-PhCCC}_6\text{H}_4(\text{CCPh})\text{-4})$ (**10b**) and reactions of **2a** with CNBu^t and $\text{CNC}_6\text{H}_3\text{Me}_2\text{-2,6}$ and **2c** and **2d** with PPh_3 are given in the ESI.†

Instrumentation

Infrared spectra were recorded on PerkinElmer System 2000 and PerkinElmer Spectrum One FT-IR spectrometers using a CaF_2 solution cell and AR grade *n*-hexane or CH_2Cl_2 solvent; spectral features are reported in cm^{-1} . ¹H NMR spectra were recorded on a Varian Gemini-300 spectrometer at 300 MHz in CDCl_3 (Cambridge Isotope Laboratories) and referenced to residual solvent (δ 7.26). ³¹P NMR spectra were recorded on a Varian Gemini-300 spectrometer at 121 MHz in CDCl_3 and referenced to external 85% H_3PO_4 . Unit resolution and high-resolution ESI mass spectra were recorded on a Micromass-Waters LC-ZMD single quadrupole liquid chromatograph-MS instrument, and are reported in the form: *m/z* (assignment, relative intensity). Microanalyses were carried out at the Microanalysis Service Unit in the Research School of Chemistry, ANU, or at the School of Human Sciences, Science Centre, London Metropolitan University, UK.

Cyclic voltammetry

Measurements were recorded at room temperature using an EA161 potentiostat and e-corder from eDAQ Pty Ltd, with platinum disk working, platinum wire auxiliary, and Ag/AgCl reference electrodes, such that the ferrocene/ferrocenium redox couple was located at 0.56 V ($i_{pc}/i_{pa} = 1$; $\Delta E_p = 0.09$ V). Scan rates were typically 100 mV s^{-1} . Solutions contained 0.1 M (N^tBu_4)PF₆ and *ca.* 10^{-3} M complex in dried, distilled dichloromethane, and were deoxygenated and maintained under a nitrogen atmosphere.

Spectroelectrochemical studies

Electronic spectra of **8b** were recorded using a Cary 5 spectrophotometer. Solution spectra of the oxidized species were obtained at 298 K by electrogeneration in a custom-built optically transparent thin-layer electrochemical (OTTLE) cell with potentials of *ca.* 200 mV beyond $E_{1/2}$ to ensure complete electrolysis. The solution was made using 0.3 M (N^tBu_4)PF₆ in dried, distilled dichloromethane under a nitrogen atmosphere.

Syntheses

Synthesis of $\text{Mo}_2\text{Ir}_3(\mu\text{-CO})_3(\text{CO})_5(\text{CNC}_6\text{H}_3\text{Me}_2\text{-2,6})(\eta^5\text{-C}_5\text{H}_5)_2(\eta^5\text{-C}_5\text{Me}_5)$ (3a**).** $\text{CNC}_6\text{H}_3\text{Me}_2\text{-2,6}$ (3.0 mg, 23.3 μmol) was added to a brown solution of $\text{Mo}_2\text{Ir}_3(\mu\text{-CO})_3(\text{CO})_6(\eta^5\text{-C}_5\text{H}_5)_2(\eta^5\text{-C}_5\text{Me}_5)$ (**1a**) (10.0 mg, 7.8 μmol) in THF (10 mL) and the resultant mixture was heated at reflux for 20 h. The solution was taken to dryness *in vacuo*, and the crude residue dissolved in the minimum amount of CH_2Cl_2 and applied to a silica pre-

parative TLC plate. Elution with CH₂Cl₂-petrol (4 : 1) afforded four bands. The contents of the first ($R_f = 0.7$, yellow), second ($R_f = 0.4$, brown) and third ($R_f = 0.2$, brown) bands were in trace amounts and were not isolated. The contents of the fourth band ($R_f = 0.1$, brown) were extracted into CH₂Cl₂, which was then reduced in volume to afford a brown solid identified as **3a** (5.9 mg, 55%). IR (CH₂Cl₂): $\nu(\text{NC})$ 2111 w, $\nu(\text{CO})$ 2003 s, 1963 w br, 1947 w sh, 1869 w, 1822 w cm⁻¹. ¹H NMR: δ 7.10–7.16 (m, 3H, C₆H₃), 5.15 (s, 5H, C₅H₅), 5.00 (s, 5H, C₅H₅), 2.41 (s, 6H, Me), 1.92 (s, 15H, C₅Me₅). MS (ESI): calc., C₃₇H₃₄Ir₃Mo₂NO₈, 1389 ([M]⁺); found, 1389 ([M]⁺, 7), 1361 ([M – CO]⁺, 5), 1333 ([M – 2CO]⁺, 14), 1305 ([M – 3CO]⁺, 35), 1277 ([M – 4CO]⁺, 100), 1249 ([M – 5CO]⁺, 16). Anal: calc. for C₃₇H₃₄Ir₃Mo₂NO₈: C 31.99, H 2.47, N 1.01%; found C 31.61, H 2.77, N 1.00%.

Synthesis of Mo₂Ir₃(μ -CO)₄(CO)₄(PPh₃)(η^5 -C₅H₅)₂(η^5 -C₅Me₅) (4a). PPh₃ (13.5 mg, 51.5 μ mol) was added to a brown solution of Mo₂Ir₃(μ -CO)₃(CO)₆(η^5 -C₅H₅)₂(η^5 -C₅Me₅) (**1a**) (14.0 mg, 10.9 μ mol) in THF (10 mL) and the resultant mixture was heated at reflux for 20 h. The solution was taken to dryness *in vacuo*, and the crude residue dissolved in the minimum amount of CH₂Cl₂ and applied to a silica preparative TLC plate. Elution with CH₂Cl₂-petrol (4 : 1) afforded two bands. The contents of the first ($R_f = 0.4$, brown) band were in trace amounts and were not isolated. The contents of the second band ($R_f = 0.2$, red-brown) were extracted into CH₂Cl₂, which was then reduced in volume to afford a red-brown solid identified as **4a** (14.2 mg, 86%). IR (CH₂Cl₂): $\nu(\text{CO})$ 2006 s, 1956 s br, 1868 w, 1771 m br, 1712 m br cm⁻¹. ¹H NMR: δ 7.58–7.43 (m, 15H, Ph), 4.80 (s, 10H, Cp), 1.84 (s, 15H, C₅Me₅). ³¹P NMR (CDCl₃): δ 19.1 (s, PPh₃). MS (ESI): calc., C₄₆H₄₀Ir₃Mo₂O₈P, 1520 ([M]⁺); found, 1559 ([M + K]⁺, 9), 1543 ([M + Na]⁺, 17), 1520 ([M]⁺, 9), 1492 ([M – CO]⁺, 10), 1464 ([M – 2CO]⁺, 37), 1436 ([M – 3CO]⁺, 35), 1408 ([M – 4CO]⁺, 47), 1380 ([M – 5CO]⁺, 100), 1352 ([M – 6CO]⁺, 46). Anal: calc. for C₄₆H₄₀Ir₃Mo₂O₁₀P: C 36.34, H 2.65%; found C 36.45, H 2.35%.

Synthesis of MoIr₄(μ -CO)₃(CO)₆(PPh₃)(η^5 -C₅H₅)(η^5 -C₅Me₅) (5a). PPh₃ (1.9 mg, 7.36 μ mol) was added to a brown solution of MoIr₄(μ -CO)₃(CO)₇(η^5 -C₅H₅)(η^5 -C₅Me₅) (**2a**) (9.9 mg, 7.36 μ mol) in CH₂Cl₂ (5 mL) and the resultant mixture was stirred for 20 h. The solution was taken to dryness *in vacuo*, and the crude residue dissolved in the minimum amount of CH₂Cl₂ and applied to a silica preparative TLC plate. Elution with CH₂Cl₂-petrol (4 : 1) afforded four bands. The contents of the first ($R_f = 0.7$, yellow) and fourth ($R_f = 0.1$, pink) bands were in trace amounts and were not isolated. The contents of the second band ($R_f = 0.6$, brown) were extracted into CH₂Cl₂ and the extract then reduced in volume, to afford an orange solid identified as MoIr₃(μ -CO)₃(CO)₆(PPh₃)₂(η^5 -C₅H₅) (2.7 mg, 48%) by MS and IR spectral comparison to an authentic sample.⁶ The contents of the third band ($R_f = 0.4$, red-brown) were extracted into CH₂Cl₂ and the extract was then reduced in volume, to afford a red-brown solid identified as **5a** (5.6 mg, 48%). IR (CH₂Cl₂): $\nu(\text{CO})$ 2056 m, 2024 w sh, 2006 sh, 1995 s, 1963 w sh, 1879 w br, 1811 w, 1767 w, 1740 m cm⁻¹. ¹H NMR: δ 7.36–7.38 (m, 15H, PPh₃), 5.01 (s, 5H, C₅H₅), 1.85 (s, 15H,

C₅Me₅). ³¹P NMR: δ 16.5 (PPh₃). MS (ESI): calc., C₄₂H₃₅Ir₄MoO₉P, 1579 ([M]⁺); found, 1579 ([M]⁺, 100). Anal: calc. for C₄₂H₃₅Ir₄MoO₉P: C 31.94, H 2.23%; found C 32.18, H 2.00%.

Synthesis of MoIr₄(μ_3 -CO)₂(μ -CO)₂(CO)₄(PPh₃)₂(η^5 -C₅H₅)(η^5 -C₅Me₅) (6). PPh₃ (2.2 mg, 8.4 mmol) was added to a solution of MoIr₄(μ -CO)₃(CO)₆(PPh₃)(η^5 -C₅H₅)(η^5 -C₅Me₅) (**5a**, 4.4 mg, 2.8 mmol) in THF (5 mL), and the resultant solution was heated at reflux for 6 h. The solution was taken to dryness *in vacuo*, and the crude residue dissolved in the minimum amount of CH₂Cl₂ and applied to a silica preparative TLC plate. Elution with CH₂Cl₂-petrol (4 : 1) afforded three bands. Bands appearing in trace amounts were not isolated. The contents of the second band ($R_f = 0.6$, red) were extracted with CH₂Cl₂ and the extracts reduced in volume to afford a red solid (0.7 mg, 16%), identified as **5a** from IR spectral comparison to an authentic sample. The contents of the third band ($R_f = 0.2$) were extracted into CH₂Cl₂, which was then reduced in volume to afford a brown solid, identified crystallographically as **6** (3.7 mg, 73%). IR (CH₂Cl₂): $\nu(\text{CO})$ 1999 m, 1974 m, 1943 m, 1870 w, 1786 w, 1734 w, 1671 w cm⁻¹. ¹H NMR: δ 7.23–7.45 (m, 30H, PPh₃), 4.49 (s, 5H, C₅H₅), 1.94 (s, 15H, C₅Me₅). ³¹P NMR: δ 33.3, –3.7 (PPh₃). MS (ESI): calc., C₅₉H₅₀Ir₄MoO₈P₂, 1818.0553 ([M]⁺); found, 1818.0544 ([M]⁺). Anal: calc. for C₅₉H₅₀Ir₄MoO₈P₂: C 39.07, H 2.78%; found C 38.97, H 2.79%.

Synthesis of Mo₂Ir₃(μ_4 - η^2 -PhC₂Ph)(μ_3 -CPh)₂(CO)₄(η^5 -C₅H₅)₂(η^5 -C₅Me₅) (7a). Diphenylacetylene (2.3 mg, 12.9 μ mol) was added to a brown solution of Mo₂Ir₃(μ -CO)₃(CO)₆(η^5 -C₅H₅)₂(η^5 -C₅Me₅) (**1a**) (16.7 mg, 13.0 μ mol) in toluene (10 mL) and the resultant mixture was heated at reflux for 1 h, monitoring by IR spectroscopy. The solution was taken to dryness *in vacuo*, and the crude residue was dissolved in the minimum amount of CH₂Cl₂ and applied to a silica preparative TLC plate. Elution with CH₂Cl₂-petrol (1 : 1) afforded four bands. The contents of the first band ($R_f = 0.7$, orange) were extracted with CH₂Cl₂ and reduced in volume to afford an orange solid, identified as **7a** (2.1 mg, 11%). IR (CH₂Cl₂): $\nu(\text{CO})$ 1992 vs, 1939 s cm⁻¹. ¹H NMR: δ 7.38–6.38 (m, 20H, Ph), 4.69 (s, 5H, Cp), 4.40 (s, 5H, Cp), 1.42 (s, 15H, C₅Me₅). MS (ESI): calc., C₅₂H₄₅Ir₃Mo₂O₄, 1502 ([M]⁺); found, 1541 ([M + K]⁺, 45), 1525 ([M + Na]⁺, 100), 1502 ([M]⁺, 51), 1474 ([M – CO]⁺, 39). Anal: calc. for C₅₂H₄₅Ir₃Mo₂O₄: C 41.57, H 3.02%; found C 41.45, H 2.74%. The contents of the second band ($R_f = 0.5$, purple) were extracted into CH₂Cl₂, which was then reduced in volume to afford a purple solid identified as **7b** (2.4 mg, 12%). IR (CH₂Cl₂): $\nu(\text{CO})$ 1993 vs, 1936 s, 1754 w, 1715 m cm⁻¹. ¹H NMR: δ 7.03–6.35 (m, 20H, Ph), 5.18 (s, 10H, C₅H₅), 1.92 (s, 15H, C₅Me₅). MS (ESI): calc., C₅₂H₄₅Ir₃Mo₂O₄, 1502 ([M]⁺); found, 1541 ([M + K]⁺, 34), 1525 ([M + Na]⁺, 100), 1502 ([M]⁺, 32), 1474 ([M – CO]⁺, 21). Anal: calc. for C₅₂H₄₅Ir₃Mo₂O₄: C 41.57, H 3.02%; found C 41.78, H 2.74%. The contents of the third band ($R_f = 0.4$, green) were extracted into CH₂Cl₂, which was then reduced in volume to afford a green solid, identified as Mo₂Ir₂(μ_4 - η^2 -PhC₂Ph)(CO)₈(η^5 -C₅H₅)₂ (0.4 mg, 3%) by IR spectral comparison to an authentic sample.⁷ The contents of the fourth band ($R_f = 0.3$, dark brown) were extracted into

CH_2Cl_2 , which was then reduced in volume to afford a brown solid, identified as unreacted $\text{Mo}_2\text{Ir}_3(\mu\text{-CO})_3(\text{CO})_6(\eta^5\text{-C}_5\text{H}_5)_2(\eta^5\text{-C}_5\text{Me}_5)$ (**1a**) (4.6 mg, 28%) by IR spectral comparison to an authentic sample.⁵

Synthesis of $\text{MoIr}_4(\mu_3\text{-}\eta^2\text{-PhC}_2\text{Ph})(\mu_3\text{-CO})_2(\text{CO})_6(\eta^5\text{-C}_5\text{H}_5)(\eta^5\text{-C}_5\text{Me}_5)$ (8a**).** Diphenylacetylene (7.0 mg, 39.3 μmol) was added to a red-brown solution of $\text{MoIr}_4(\mu\text{-CO})_3(\text{CO})_7(\eta^5\text{-C}_5\text{H}_5)(\eta^5\text{-C}_5\text{Me}_5)$ (**2a**) (4.5 mg, 3.3 μmol) in CH_2Cl_2 (5 mL) and the resultant mixture was heated at reflux for 3 h, the extent of reaction being monitored by IR spectroscopy. The solution was taken to dryness *in vacuo*, and the crude residue dissolved in the minimum amount of CH_2Cl_2 and applied to a silica preparative TLC plate. Elution with CH_2Cl_2 –petrol (1 : 1) afforded one band ($R_f = 0.30$, brown); extraction into CH_2Cl_2 and reduction in volume of the extract afforded a brown solid identified as **8a** (4.0 mg, 82%). IR (CH_2Cl_2): $\nu(\text{CO})$ 2034 vw, 2015 s, 1999 s, 1977 w, 1943 w, 1682 m, 1671 w cm^{-1} . ^1H NMR: δ 7.06–6.78 (m, 10H, Ph), 5.45 (s, 5H, Cp), 1.99 (s, 15H, C_5Me_5). MS (ESI): calc., $\text{C}_{37}\text{H}_{30}\text{Ir}_4\text{MoO}_8$, 1468 ($[\text{M}]^+$); found, 1507 ($[\text{M} + \text{K}]^+$, 54), 1491 ($[\text{M} + \text{Na}]^+$, 100), 1468 ($[\text{M}]^+$, 69). Anal: calc. for $\text{C}_{37}\text{H}_{30}\text{Ir}_4\text{MoO}_8$: C 30.28, H 2.06%; found C 30.11, H 1.90%.

Synthesis of $\text{WIr}_4(\mu_3\text{-}\eta^2\text{-PhC}_2\text{C}_6\text{H}_4(\text{C}\equiv\text{CPh})\text{-3})(\mu_3\text{-CO})_2(\text{CO})_6(\eta^5\text{-C}_5\text{H}_5)(\eta^5\text{-C}_5\text{Me}_5)$ (9a**).** 1,3-Bis(phenylethynyl)benzene (2.0 mg, 7.2 μmol) was added to a solution of $\text{WIr}_4(\mu\text{-CO})_3(\text{CO})_7(\eta^5\text{-C}_5\text{H}_5)(\eta^5\text{-C}_5\text{Me}_5)$ (**2b**) (10.0 mg, 7.0 μmol) in CH_2Cl_2 , and the resultant solution heated at reflux for 17 h, the extent of reaction being monitored by IR spectroscopy. The solution was taken to dryness *in vacuo*, and the crude residue dissolved in the minimum amount of CH_2Cl_2 and applied to a silica preparative TLC plate. Elution with CH_2Cl_2 –petrol (3 : 1) afforded at least six bands; bands appearing in trace amounts were not isolated. The contents of the fifth band ($R_f = 0.2$, green) were extracted with CH_2Cl_2 and the extracts reduced in volume to afford a green solid, identified as **9a** (5.2 mg, 44%). IR (*n*-hexane): $\nu(\text{CO})$ 2040 w, 2025 vs, 2006 s, 1983 m, 1952 w, 1692 w, 1673 m cm^{-1} . ^1H NMR: δ 7.51–6.77 (m, 14H, $\text{C}_6\text{H}_4 + \text{Ph}$), 5.60 (s, 5H, C_5H_5), 1.89 (s, 15H, C_5Me_5). MS (ESI): calculated, $\text{C}_{45}\text{H}_{35}\text{Ir}_4\text{O}_8\text{W}$, 1659.0359 ($[\text{M} + \text{H}]^+$); found, 1659.0354 ($[\text{M} + \text{H}]^+$). Slow decomposition of **9a** precluded elemental analysis.

Synthesis of $[\text{WIr}_4(\mu_3\text{-CO})_2(\text{CO})_6(\eta^5\text{-C}_5\text{H}_5)(\eta^5\text{-C}_5\text{Me}_5)]_2(\mu_6\text{-}\eta^4\text{-PhC}_2\text{C}_6\text{H}_4(\text{C}_2\text{Ph})\text{-3})$ (10a**).** 1,3-Bis(phenylethynyl)benzene (1.0 mg, 3.6 μmol) was added to a solution of $\text{WIr}_4(\mu\text{-CO})_3(\text{CO})_7(\eta^5\text{-C}_5\text{H}_5)(\eta^5\text{-C}_5\text{Me}_5)$ (**2b**) (10.0 mg, 7.0 μmol) in CH_2Cl_2 , and the resultant solution was heated at reflux for 19 h, the extent of reaction being monitored by IR spectroscopy. The solution was taken to dryness *in vacuo*, and the crude residue dissolved in the minimum amount of CH_2Cl_2 and applied to a silica preparative TLC plate. Elution with CH_2Cl_2 –petrol (3 : 1) afforded at least six bands; bands appearing in trace amounts were not isolated. The contents of the fifth band ($R_f = 0.2$, green) were extracted with CH_2Cl_2 and the extracts reduced in volume to afford a green solid, identified as **9a** (4.0 mg, 2.4 μmol , 34%) by IR spectroscopic comparison with an authentic sample. The baseline was collected, extracted with CH_2Cl_2 and re-applied to a silica preparative TLC plate.

Elution with acetone–petrol (2 : 3) afforded two bands; the contents of the first band ($R_f = 0.5$, green) occurred in trace amounts and were not isolated. The contents of the second and major band ($R_f = 0.4$, green) were extracted into CH_2Cl_2 , which was then reduced in volume to afford a green solid, identified as **10a** (1.6 mg, 7%). IR (CH_2Cl_2): $\nu(\text{CO})$ 2035 w sh, 2015 s, 2002 s, 1976 m, 1944 w, 1682 w, 1662 w br cm^{-1} . MS (ESI): calculated, $\text{C}_{68}\text{H}_{54}\text{Ir}_8\text{O}_{16}\text{W}_2$, 3037.9466 ($[\text{M}]^+$); found, 3037.9460 ($[\text{M}]^+$). The low yield precluded NMR spectroscopic and microanalytical analysis.

X-ray crystallographic studies

General. The crystal and refinement data for compounds **3a**, **4a–4c**, **5b**, **6**, **7a**, **8a**, **8b** and **9a** are summarized in Table S1.† Crystals suitable for the X-ray structural analyses were grown by liquid diffusion of methanol into a dichloromethane solution (**3a**, **4b**, **4c**, **8b**, **9a**), liquid diffusion of ethanol into a dichloromethane solution (**4a**, **7a**, **8a**), liquid diffusion of methanol into a chloroform solution (**5b**) or liquid diffusion of hexane into a dichloromethane solution (**6**) at 277 K. Suitable crystals were mounted on fine glass capillaries, and intensity data were collected on a Nonius KAPPA CCD diffractometer at 200 K using graphite-monochromated Mo- $\text{K}\alpha$ radiation ($\lambda = 0.71073 \text{ \AA}$). N_t (total) reflections were measured by using psi and omega scans and were reduced to N_o unique reflections, with $F_o > 2\sigma(F_o)$ being considered to be observed. Data were initially processed and corrected for absorption by using the programs DENZO⁸ and SORTAV.⁹ The structures were solved using direct methods and observed reflections were used in least-squares refinement on F^2 , with anisotropic thermal parameters refined for non-hydrogen atoms. Hydrogen atoms were constrained in calculated positions and refined with a riding model. Structure solutions and refinements were performed by using the CRYSTALS¹⁰ software package or the programs SHELXS-97 and SHELXL-97¹¹ through the graphical interface Olex2,¹² which was also used to generate the figures. In all structures, the largest peaks in the final difference electron map are located near the metal atoms. Crystallographic data for the structural analyses have been deposited with the Cambridge Crystallographic Data Centre, CCDC numbers 1018833–1018842.

Variata. **4a.** Disordered lattice solvent could not be successfully modelled, so was removed from the refinement using PLATON SQUEEZE.¹³ **4b.** Anisotropic displacement parameter restraints were applied to phenyl rings C21–C26, C27–C32 and C33–C38 of the triphenylphosphine moiety. Disordered lattice solvent could not be successfully modelled and was therefore removed from the refinement using PLATON SQUEEZE.¹³ **6.** The asymmetric unit contains two cluster molecules and three molecules of dichloromethane. The Flack¹⁴ parameter refined to 0.491(8) indicating a nearly 50 : 50 inversion twin. A check in PLATON ADDSYM¹⁵ confirmed that no additional symmetry elements needed to be added to the space group, and thus Pca_21 was the most suitable space group. Bond distance restraints were applied to the two pentamethylcyclopentadienyl ligands and the three lattice

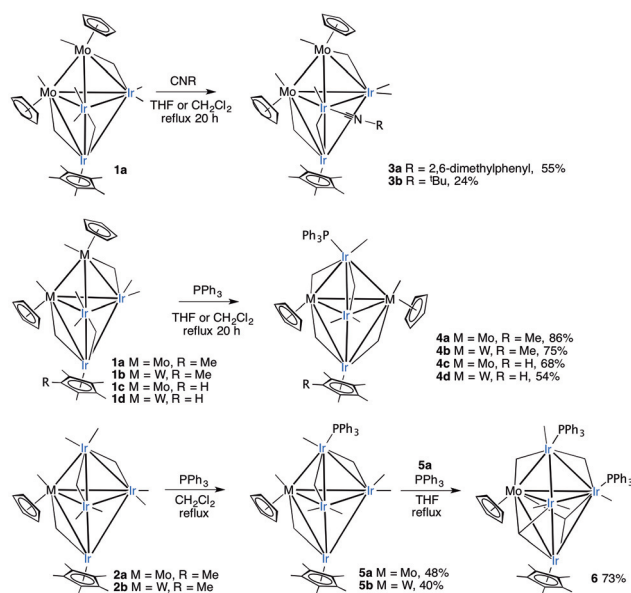
dichloromethane molecules. Anisotropic displacement parameter restraints were applied to atoms C222, O222, C551, O551, C881 and O881 (carbonyl ligands) and the cyclopentadienyl and triphenylphosphine ligands. **7a**. The asymmetric unit contains one and a half cluster molecules; the second cluster molecule is generated through a mirror plane that passes through Mo6, Ir8 and Mo9. Disordered lattice solvent could not be successfully modelled and was therefore removed from the refinement using PLATON SQUEEZE.¹³ **8a**. The Cp ligand (C1–C5) exhibited positional disorder. This was successfully modelled using a two-level model with 0.51(0.01):0.49 occupancy levels, in conjunction with anisotropic displacement parameter restraints. **6b**. The asymmetric unit contains one cluster molecule, and two half molecules of dichloromethane. The Cp ligand (C1–C5) exhibited positional disorder, successfully modelled using a two-level model with 0.59(0.01):0.41 occupancy levels, in conjunction with anisotropic displacement parameter restraints. Anisotropic displacement parameter restraints were also applied to the lattice dichloromethane molecules. **9a**. Anisotropic displacement parameter restraints were applied to atoms C16–C37 (alkyne ligand), atoms C1–C5, C6–C15 (Cp ligands), and the C and O atoms of all carbonyl ligands. Disordered lattice solvent could not be successfully modelled and was therefore removed from the refinement using PLATON SQUEEZE.¹³

Results and discussion

Syntheses and spectroscopic characterization of 3–6

The reaction of $\text{Mo}_2\text{Ir}_3(\mu\text{-CO})_3(\text{CO})_6(\eta^5\text{-C}_5\text{H}_5)_2(\eta^5\text{-C}_5\text{Me}_5)$ (**1a**) with three equivalents of 2,6-dimethylphenyl isocyanide or *t*-butyl isocyanide in refluxing THF or CH_2Cl_2 led to the substitution of one carbonyl ligand from one of the less-sterically-hindered iridium atoms and the subsequent formation of **3a** and **3b**, isolated as brown solids after preparative TLC in yields of 55 and 24%, respectively (Scheme 1). **3a** and **3b** exhibit $\nu(\text{CN})$ bands in the solution IR spectra at 2111 and 2146 cm^{-1} , respectively, while the ESI mass spectra of **3a** and **3b** reveal molecular ion peaks with the correct characteristic isotope pattern at 1389 and 1347 mass units, respectively. The molecular structure of **3a** was determined by a single-crystal X-ray diffraction study (see below), with that of **3b** presumed similar due to the spectral similarities. In contrast to these observations, $\text{MoIr}_4(\mu\text{-CO})_3(\text{CO})_7(\eta^5\text{-C}_5\text{H}_5)(\eta^5\text{-C}_5\text{Me}_5)$ (**2a**) reacted with three equivalents of *t*-butyl isocyanide or five equivalents of 2,6-dimethylphenyl isocyanide with loss of the $\text{Ir}(\eta^5\text{-C}_5\text{Me}_5)$ vertices to give $\text{MoIr}_3(\mu\text{-CO})_3(\text{CNR})(\text{CO})_7(\eta^5\text{-C}_5\text{H}_5)$.

Reaction of **1a** with an excess of PPh_3 in refluxing THF for 20 h led to the formation of **4a**, which was isolated by preparative TLC as a red/brown solid in 86% yield (Scheme 1). Similar reactions of **1b–1d** with PPh_3 in either refluxing CH_2Cl_2 or refluxing THF afforded **4b–4d** in good yields. The new clusters were characterized by IR, ^1H and ^{31}P NMR spectroscopies, ESI MS, satisfactory microanalyses and, in the case of **4a–4c**, single-crystal X-ray diffraction studies. The IR spectra of **4a–4d**



Scheme 1 Syntheses of 3–6.

in CH_2Cl_2 are analogous, with five $\nu(\text{CO})$ bands spanning the range 2006–1708 cm^{-1} ; the close visual similarity of the IR spectra is suggestive of isostructural species. The ^1H NMR spectra of **4a** and **4c** each possess a single resonance for the two cyclopentadienyl ligands, consistent with a symmetrical structure for the clusters, whereas those of **4b** and **4d** each contain two cyclopentadienyl resonances. The ^{31}P NMR spectra reveal singlet resonances for each cluster that move downfield on proceeding from co-ligand C_5Me_5 to $\text{C}_5\text{Me}_4\text{H}$ and on replacing tungsten with molybdenum. The ESI mass spectra each show a molecular ion with the correct characteristic isotope pattern (see Fig. S1† for a representative ESI MS molecular ion and its sodium adduct and their calculated counterparts (those of **4d**)).

Addition of one equivalent of PPh_3 to **2a** or **2b** afforded the phosphine-substituted products $\text{M}\text{Ir}_4(\mu\text{-CO})_3(\text{CO})_6(\text{PPh}_3)(\eta^5\text{-C}_5\text{H}_5)(\eta^5\text{-C}_5\text{Me}_5)$ ($\text{M} = \text{Mo}$ **5a**, $\text{M} = \text{W}$ **5b**), isolated following preparative TLC in yields of 48% and 40%, respectively. Clusters **5a** and **5b** have been characterized by IR, ^1H and ^{31}P NMR spectroscopies, ESI mass spectrometry and, in the case of **5b**, a single-crystal X-ray diffraction study. The solution IR spectra of **5a** and **5b** contain nine $\nu(\text{CO})$ bands, six of which correspond to terminally bound carbonyls (2056–1879 cm^{-1}) and three to bridging carbonyl modes (1821–1727 cm^{-1}). As is the case with **4a–4d**, the similarity in the spectra of **5a** and **5b** is suggestive of isostructural clusters. The ^1H NMR spectra of **5a** and **5b** contain signals due to the Cp and Cp* ligands and the phenyl groups of the triphenylphosphine unit, as expected, while **5a** and **5b** show signals in the ^{31}P NMR spectrum at δ 16.5 and 13.0, respectively, due to the triphenylphosphine ligand. The ESI mass spectra of **5a** and **5b** confirm the cluster composition with peaks showing the characteristic isotope pattern at 1579 ($[\text{M}]^+$) and 1670 ($[\text{M} + \text{Na}]^+$) mass units, respectively. In contrast

to these observations, reactions of PPh_3 with the tetramethylcyclopentadienyl-ligated clusters **2c** and **2d** under the same conditions did not afford any identifiable cluster species.

Amongst the products obtained following the addition of one equivalent of PPh_3 to a solution of **2a** was the previously reported tetranuclear cluster $\text{MoIr}_3(\mu\text{-CO})_3(\text{CO})_6(\text{PPh}_3)_2(\eta^5\text{-C}_5\text{H}_5)$.⁶ To explore the possibility that *in situ* attack of **5a** by a second equivalent of PPh_3 led to the displacement of the $\text{Ir}(\eta^5\text{-C}_5\text{Me}_5)$ group, and subsequent formation of the bis-substituted tetranuclear product, a sample of **5a** was treated with one equivalent of PPh_3 in CH_2Cl_2 at room temperature, but no change was observed after 24 h. Similarly, addition of excess PPh_3 had no noticeable effect. When **5a** was heated in refluxing THF for 6 h with three equivalents of PPh_3 , however, a new species began to form, which was isolated as a brown solid in 73% yield, and identified as the bis-substituted pentanuclear cluster $\text{MoIr}_4(\mu\text{-CO})_3(\text{CO})_5(\text{PPh}_3)_2(\eta^5\text{-C}_5\text{H}_5)(\eta^5\text{-C}_5\text{Me}_5)$ (**6**) (Scheme 1), ruling out the possibility of **6** being an intermediate in the formation of $\text{MoIr}_3(\mu\text{-CO})_3(\text{CO})_6(\text{PPh}_3)_2(\eta^5\text{-C}_5\text{H}_5)$. The solution IR spectrum of **6** contains seven $\nu(\text{CO})$ bands, four of which correspond to terminally bound carbonyls ($1999\text{--}1870\text{ cm}^{-1}$) and three to bridging/face-capping carbonyl modes ($1786\text{--}1671\text{ cm}^{-1}$). The ^1H NMR spectrum of **6** is as expected, while the ^{31}P NMR spectrum shows two signals at δ 33.3 and -3.7 (note that the ^{31}P NMR chemical shifts are not a definitive indicator of ligation site in Mo/W–Ir clusters, spectral assignment of which necessitates further studies: see, for example, ref. 4e). The ESI mass spectrum of **6** reveals a peak with the correct characteristic isotope pattern at 1818 ($[\text{M}]^+$). The structure of **6** was conclusively established from a single-crystal X-ray diffraction study.

X-ray structural studies of **3a**, **4a–4c**, **5b**, and **6**

Single-crystal X-ray diffraction studies confirmed the molecular compositions of **3a**, **4a–4c**, **5b**, and **6**. ORTEP plots with the molecular structure and atomic labeling schemes for **3a**, **4a**, **5b**, and one of the two crystallographically distinct molecules of **6** are shown in Fig. 1–4, respectively. Fig. S2–S4† contain ORTEP plots from the structural studies of **4b** and **4c**, and the remaining crystallographically independent molecule of **6**, respectively; **4b** and **4c** are isostructural with **4a**. Table S1 in the ESI† contains crystallographic data acquisition and refinement parameters, Table 1 lists selected bond distances for **4a–4c**, with selected bond distances for **3a**, **5b**, and the two molecules of **6** being given in the respective figure captions.

The metal cores of **3a**, **4a–4c**, **5b**, and **6** possess trigonal bipyramidal geometries with the group 6 metal atom(s) and one of the iridium atoms ligated by η^5 -cyclopentadienyl ligands with varying degrees of alkylation. Whereas **3a**, **5b**, and **6** possess the same core metal disposition as their starting clusters, the cores of **4a–4c** result from a formal isomerization corresponding to interchange of an apical Mo/W and equatorial Ir. The structural studies reveal that the incoming ligand is coordinated at equatorial (**3a**), apical (**4a–4c**, **5b**), and equatorial and apical (**6**) iridium atoms. The clusters contain five (**3a**), four (**4a–4c**, **6**) or six (**5b**) terminal carbonyls, three (**3a**, **5b**),

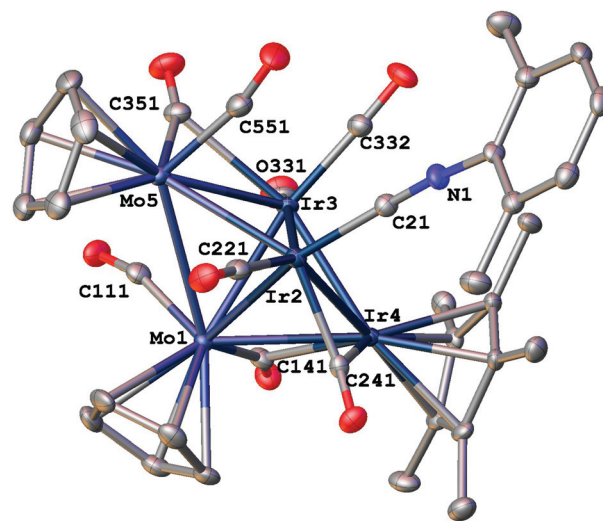


Fig. 1 ORTEP plot and atom numbering scheme for $\text{Mo}_2\text{Ir}_3(\mu\text{-CO})_3(\text{CO})_5(\text{CNC}_6\text{H}_5\text{Me}_2\text{-}2,6)(\eta^5\text{-C}_5\text{H}_5)_2(\eta^5\text{-C}_5\text{Me}_5)$ (**3a**). Displacement ellipsoids are shown at the 40% probability level. Hydrogen atoms and lattice dichloromethane molecule have been omitted for clarity. Selected bond lengths: Mo1–Ir2 2.7670(5), Mo1–Ir3 2.8147(5), Mo1–Ir4 2.8349(5), Mo1–Mo5 3.0536(7), Ir2–Ir3 2.7209(3), Ir2–Ir4 2.7369(3), Ir2–Mo5 2.8490(6), Ir3–Ir4 2.6859(3), Ir3–Mo5 2.7871(5), Mo1–C111 1.976(7), Mo1–C141 1.966(6), Ir2–C21 1.967(6), Ir2–C221 1.881(6), Ir2–C241 1.994(6), Ir3–C331 1.859(6), Ir3–C332 1.870(6), Ir3–C351 2.456(7), Ir4–C141 2.375(6), Ir4–C241 2.049(6), Mo5–C351 1.986(7), Mo5–C551 1.991(7), N1–C21 1.168(8) Å.

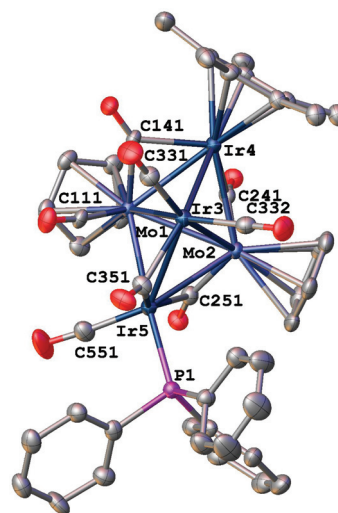


Fig. 2 ORTEP plot and atom numbering scheme for $\text{Mo}_2\text{Ir}_3(\mu\text{-CO})_4(\text{CO})_4(\text{PPh}_3)(\eta^5\text{-C}_5\text{H}_5)_2(\eta^5\text{-C}_5\text{Me}_5)$ (**4a**). Displacement ellipsoids are shown at the 40% probability level. Hydrogen atoms have been omitted for clarity.

four (**4a–4c**), or two (**6**) bridging carbonyls, and, in the case of **6**, two face-capping carbonyl ligands. All possess 72 cluster valence electrons, and so are EAN-precise for M_5 clusters with nine M–M bonds. While the core bond distances fall within the range of literature precedents, the M1–Ir5 (**4a–4c**) and

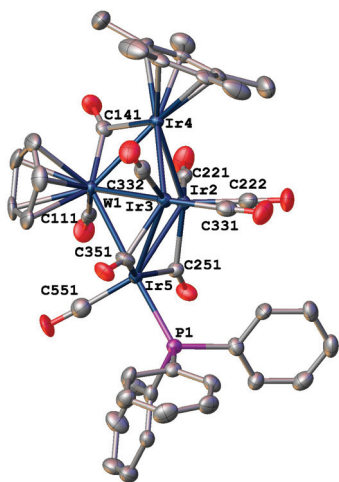


Fig. 3 ORTEP plot and atom numbering scheme for $\text{WIr}_4(\mu\text{-CO})_3\text{-(CO)}_6(\text{PPh}_3)(\eta^5\text{-C}_5\text{H}_5)(\eta^5\text{-C}_5\text{Me}_5)$ (**5b**). Displacement ellipsoids are shown at the 40% probability level. Hydrogen atoms and lattice chloroform molecule have been omitted for clarity. Selected bond lengths: W1–Ir2 2.8474(6), W1–Ir3 2.7710(6), W1–Ir4 2.7284(5), W1–Ir5 2.8677(5), Ir2–Ir3 2.7130(5), Ir2–Ir4 2.7621(5), Ir2–Ir5 2.7828(5), Ir3–Ir4 2.7118(5), Ir3–Ir5 2.7937(5), W1–C111 1.984(13), W1–C141 2.085(11), Ir2–C221 1.891(11), Ir2–C222 1.883(14), Ir2–C251 2.057(10), Ir3–C331 1.933(14), Ir3–C332 1.857(12), Ir3–C351 2.090(11), Ir4–C141 2.079(11), Ir5–C251 2.146(10), Ir5–C351 2.064(13), Ir5–C551 1.863(13), Ir5–P1 2.337(3) Å.

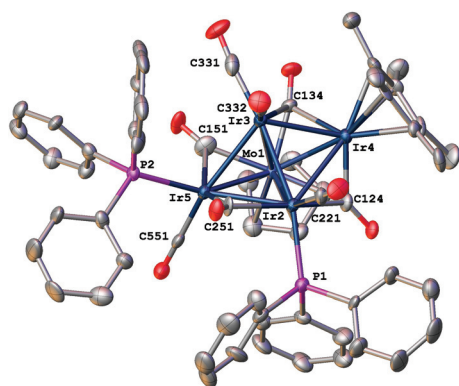


Fig. 4 ORTEP plot and atom numbering scheme for one of the two crystallographically distinct molecules of $\text{MoIr}_4(\mu_3\text{-CO})_2(\mu\text{-CO})_2\text{-(CO)}_4(\text{PPh}_3)_2(\eta^5\text{-C}_5\text{H}_5)(\eta^5\text{-C}_5\text{Me}_5)$ (**6**). Displacement ellipsoids are shown at the 40% probability level. Hydrogen atoms and lattice dichloromethane molecules have been omitted for clarity. Selected bond lengths: Mo1–Ir2 2.9194(13), Mo1–Ir3 2.7914(13), Mo1–Ir4 2.8359(13), Mo1–Ir5 2.7743(13), Ir2–Ir3 2.7023(7), Ir2–Ir4 2.8145(8), Ir2–Ir5 2.7737(7), Ir3–Ir4 2.6830(8), Ir3–Ir5 2.7379(8), Mo1–C124 2.656(15), Mo1–C134 1.978(15), Mo1–C151 2.102(19), Ir2–C124 2.157(13), Ir2–C221 1.881(15), Ir2–C251 2.164(12), Ir2–P1 2.369(4), Ir3–C134 2.522(15), Ir3–C331 1.86(2), Ir3–C332 1.857(16), Ir4–C124 1.972(15), Ir4–C134 2.430(15), Ir5–C151 2.197(16), Ir5–C251 2.065(14), Ir5–C551 1.835(16), Ir5–P2 2.335(4) Å.

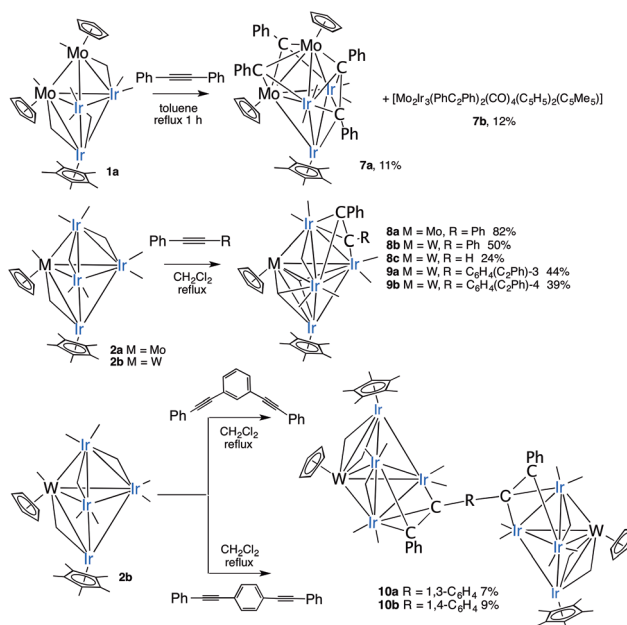
Ir1–W5 (**5b**) bonds are the longest M–Ir vectors in these structures, consistent with their trans dispositions to the incoming PPh_3 ligand.

Table 1 Selected bond lengths (Å) for **4a–4c**

	4a M = Mo	4b M = W	4c M = Mo
M1–M2	2.9622(7)	2.9399(13)	2.9553(9)
M1–Ir3	2.8420(5)	2.8330(8)	2.8246(7)
M1–Ir4	2.7926(5)	2.7813(11)	2.8235(9)
M1–Ir5	2.8406(6)	2.8305(8)	2.8713(7)
M2–Ir3	2.8015(5)	2.7968(10)	2.8180(8)
M2–Ir4	2.8194(6)	2.8154(8)	2.7644(7)
M2–Ir5	2.8573(5)	2.8606(10)	2.8425(7)
Ir3–Ir4	2.7652(3)	2.7683(8)	2.7656(6)
Ir3–Ir5	2.7706(3)	2.7731(10)	2.7148(6)
M1–C111	1.993(6)	2.010(10)	1.969(6)
M1–C141	2.053(6)	2.019(10)	2.064(6)
M2–C241	1.997(7)	1.992(9)	1.994(5)
M2–C251	1.992(7)	2.002(10)	1.985(6)
Ir3–C331	1.914(7)	1.903(10)	1.913(6)
Ir3–C332	1.865(7)	1.875(12)	1.865(6)
Ir3–C351	2.125(6)	2.123(10)	2.171(6)
Ir4–C141	2.096(6)	2.065(9)	2.046(5)
Ir4–C241	2.261(6)	2.319(10)	2.301(6)
Ir5–C551	1.845(7)	1.862(11)	1.859(6)
Ir5–C251	2.396(6)	2.411(10)	2.481(6)
Ir5–C351	2.011(6)	2.000(10)	1.990(6)
Ir5–P1	2.3134(16)	2.316(3)	2.3155(14)

Syntheses and spectroscopic characterization of **7–10**

Reaction of one equivalent of diphenylacetylene with **1a** proceeded in refluxing toluene over one hour, affording two main products that were isolated following preparative TLC in yields of 11% (**7a**) and 12% (**7b**) (Scheme 2). An X-ray structural study of a single crystal of **7a** identified the compound as $\text{Mo}_2\text{Ir}_3(\mu_4\text{-}\eta^2\text{-PhC}_2\text{Ph})(\mu_3\text{-CPh})_2(\text{CO})_4(\eta^5\text{-C}_5\text{H}_5)_2(\eta^5\text{-C}_5\text{Me}_5)$ (**7a**) (Fig. 5); its ESI mass spectrum and ^1H NMR spectroscopy data are consistent with this formulation. From a comparison



Scheme 2 Syntheses of **7–10**.

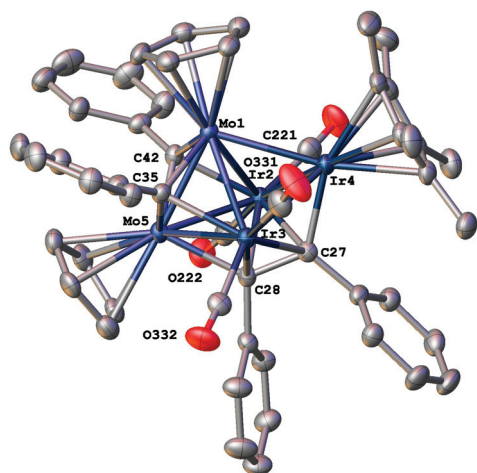


Fig. 5 ORTEP plot and atom numbering scheme for one of the two crystallographically distinct molecules of $\text{Mo}_2\text{Ir}_3(\mu_4\text{-}\eta^2\text{-PhC}_2\text{Ph})(\mu_3\text{-CPh})_2(\text{CO})_4(\eta^5\text{-C}_5\text{H}_5)_2(\eta^5\text{-C}_5\text{Me}_5)$ (**7a**). Displacement ellipsoids are shown at the 40% probability level. Hydrogen atoms have been omitted for clarity. Selected bond lengths: Mo1–Ir2 2.8968(4), Mo1–Ir3 2.8429(5), Mo1–Ir4 2.6969(4), Mo1–Mo5 2.6016(6), Ir2–Ir4 2.7636(3), Ir2–Mo5 2.8014(4), Ir3–Ir4 2.7664(3), Ir3–Mo5 2.8377(4), Mo1–C35 2.065(5), Mo1–C42 2.047(5), Ir2–C221 1.865(6), Ir2–C222 1.887(6), Ir2–C27 2.352(5), Ir2–C28 2.291(5), Ir2–C42 2.164(4), Ir3–C331 1.855(6), Ir3–C332 1.896(5), Ir3–C27 2.319(5), Ir3–C28 2.284(5), Ir3–C35 2.148(5), Ir4–C27 2.048(5), Mo5–C28 2.182(5), Mo5–C35 2.041(5), Mo5–C42 2.064(5), C27–C28 1.472(6) Å.

of the IR, ^1H NMR, and ESI mass spectral data, the second product (**7b**) is proposed to be an isomer of **7a**. The solution IR spectrum of **7a** in CH_2Cl_2 contains only two $\nu(\text{CO})$ bands, both corresponding to terminally-bound carbonyls (1992 and 1939 cm^{-1}). In contrast, that of **7b** contains four $\nu(\text{CO})$ bands, two corresponding to terminally-bound carbonyls (1993 and 1936 cm^{-1}) and two corresponding to face-capping carbonyl modes (1754 and 1715 cm^{-1}). The ^1H NMR spectrum of **7a** contains two resonances for the two cyclopentadienyl groups at δ 4.69 and 4.40, while that of **7b** contains a single resonance for the two cyclopentadienyl groups at δ 5.18; for both clusters, the phenyl, cyclopentadienyl, and pentamethyl-cyclopentadienyl protons are found in the ratio 20:10:15 (4Ph:2Cp:1Cp*). The ESI mass spectra of both clusters contain intense molecular ion peaks at 1502 ($[\text{M}]^+$), in addition to sodium and potassium adducts of the molecular ion at 1525 and 1541 mass units, respectively. While the data are suggestive of isomers, attempts to interconvert the species, both photochemical (short and long wavelength lamps) and thermal (refluxing toluene, 16 h), were unsuccessful, unreacted **7a** and **7b** being recovered and confirmed by IR. This result, coupled with the ambiguity of the existing spectral data, and our inability thus far to obtain suitable single crystals for an X-ray diffraction study, renders further speculation of the identity of **7b** unwarranted.

Reactions of more than one equivalent of arylalkynes with **2a** or **2b** proceeded under milder conditions (refluxing CH_2Cl_2) than the aforementioned reaction with **1a**, affording **8a–8c**, **9a**,

and **9b** in fair to good yields and **10a** and **10b** in poor yields (Scheme 2), the products being isolated following preparative TLC as brown (**8a**) or green solids and characterized by IR and ^1H NMR spectroscopy and HR-ESI mass spectrometry, and, in the case of **8a**, **8b**, and **9a**, single-crystal X-ray diffraction studies. Five $\nu(\text{CO})$ bands ($2041\text{--}1943\text{ cm}^{-1}$) corresponding to terminally bound carbonyl ligands are observed in the solution IR spectra; the IR spectra also display two weak bands corresponding to face-capping carbonyl modes. The ESI mass spectra contain molecular ions (**8a–8c**, **10a**, **10b**) or protonated molecular ions (**9a**, **9b**) with the correct isotope pattern.

X-ray structural studies of **7a**, **8a**, **8b**, and **9a**

Single-crystal X-ray diffraction studies revealed the molecular compositions of **7a**, **8a**, **8b**, and **9a**. ORTEP plots with the molecular structure and atomic labeling schemes for one of the two crystallographically distinct molecules of **7a** and the molecule of **9a** are shown in Fig. 5 and 6, respectively. Fig. S5–S7 in the ESI† contain ORTEP plots from the structural studies of the remaining crystallographically independent molecule of **7a**, and the molecules of **8a** and **8b**, respectively; the connectivity of the cluster cores of **8a** and **8b** mimic that of **9a**. Table S1 in the ESI† contains crystallographic data acquisition and refinement parameters, and Table 2 lists selected bond distances for **8a**, **8b**, and **9a**, while selected bond distances for the two molecules of **7a** are given in the relevant figure caption.

The metal core of **7a** adopts a distorted square-based pyramidal geometry in which one of the equatorial Ir–Ir bonds from the trigonal bipyramidal precursor has been cleaved (Ir2...Ir3 = 3.698 \AA). As with **3a**, **5b** and **6**, the metal cores of **8a**, **8b**, and **9a** possess trigonal bipyramidal geometries with the same core metal disposition as their starting clusters. In the structures of **7a**, **8a**, **8b**, and **9a**, the group 6 metal atom(s) and one of the iridium atoms are ligated by η^5 -cyclopenta-

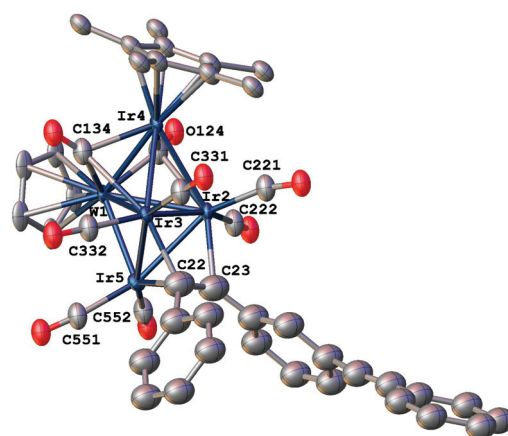


Fig. 6 ORTEP plot and atom numbering scheme for $\text{WIr}_4(\mu_3\text{-}\eta^2\text{-PhC}_2\text{C}_6\text{H}_4(\text{C}\equiv\text{CPh})\text{-}3)(\mu_3\text{-CO})_2(\text{CO})_6(\eta^5\text{-C}_5\text{H}_5)(\eta^5\text{-C}_5\text{Me}_5)$ (**9a**). Displacement ellipsoids are shown at the 40% probability level. Hydrogen atoms have been omitted for clarity.

Table 2 Selected bond lengths (Å) for **8a**, **8b** and **9a**

	8a : M = Mo	8b : M = W	9a : M = W
M1–Ir2	2.9333(9)	2.9485(5)	2.9161(13)
M1–Ir3	2.8949(9)	2.8741(5)	2.9134(12)
M1–Ir4	2.6904(10)	2.6836(5)	2.6728(13)
M1–Ir5	2.6443(9)	2.6299(5)	2.6276(12)
Ir2–Ir3	2.6026(5)	2.6066(4)	2.5952(13)
Ir2–Ir4	2.8075(5)	2.8211(5)	2.8171(14)
Ir2–Ir5	2.6957(5)	2.6869(5)	2.6907(13)
Ir3–Ir4	2.8479(5)	2.8658(5)	2.8456(13)
Ir3–Ir5	2.7119(5)	2.7059(5)	2.6959(13)
M1–C124	2.030(11)	2.015(10)	2.05(2)
M1–C134	2.051(12)	2.034(9)	2.06(3)
Ir2–C221	1.924(11)	1.921(10)	1.87(2)
Ir2–C222	1.905(12)	1.895(10)	1.93(3)
Ir2–C124	2.532(10)	2.606(9)	2.52(3)
Ir2–C23	2.148(10)	2.104(9)	2.22(3)
Ir3–C331	1.938(12)	1.935(9)	1.87(2)
Ir3–C332	1.892(12)	1.895(10)	1.83(2)
Ir3–C134	2.517(12)	2.530(10)	2.63(3)
Ir3–C22	2.131(9)	2.087(9)	2.08(3)
Ir4–C124	2.116(10)	2.158(8)	2.12(2)
Ir4–C134	2.138(10)	2.126(8)	2.17(2)
Ir5–C551	1.860(13)	1.877(10)	1.94(3)
Ir5–C552	1.877(11)	1.847(10)	1.83(2)
Ir5–C22	2.206(9)	2.208(8)	2.21(3)
Ir5–C23	2.182(10)	2.220(8)	2.24(4)
C22–C23	1.343(14)	1.426(12)	1.46(5)

dienyl ligands with varying degrees of alkylation. The clusters contain four (**7a**) or six (**8a**, **8b**, **9a**) terminal carbonyls, and, for the latter, two face-capping carbonyl ligands. The structural studies reveal that alkyne ligands are coordinated in a classic $\mu_3\text{-}\eta^2$ -“parallel” fashion across an Ir_3 face in **8a**, **8b**, and **9a**, the face that is least sterically hindered, and in a $\mu_4\text{-}\eta^2$ -fashion in **7a** oriented perpendicular to the non-bonding Ir2–Ir3 vector; for the latter, phenylmethylidyne residues resulting from $\text{C}\equiv\text{C}$ cleavage cap the Mo_2Ir faces. Assuming four electrons contributed to each cluster from the alkyne ligands and three from each alkylidyne moiety, **8a**, **8b**, and **9a** possess 72 cluster valence electrons, EAN-precise for M_5 clusters with nine M–M bonds. Alternatively, considering the alkyne carbon atoms in **8a**, **8b**, and **9a** as core atoms, the cores of **8a**, **8b**, and **9a** can be described from the condensed polyhedra perspective as square-based pyramids (74 CVE) fused *via* a triangular face (–48 CVE) to a trigonal bipyramid (72 CVE) with two main group atoms within the cores (–2 × 10 CVE) = 78 CVE, consistent with the electron count ($1 \times 6(\text{M}) + 4 \times 9(\text{Ir}) + 2 \times 4(\text{core C}) + 2 \times 5(\text{Cp/Cp}^*) + 8 \times 2(\text{CO}) + 2 \times 1(\text{Ph})$). In contrast, **7a** possesses 72 CVE, which is two electrons deficient for an M_5 cluster with 8 M–M bonds. Alternatively, one can view **7a** as a bicapped (PhC_{35} , PhC_{42}) pentagonal bipyramid (apices Ir2, Ir3, and equatorial atoms Mo1, Ir4, C27, C28, Mo5); the condensed polyhedra-predicted count for a pentagonal bipyramid (100 CVE) with two main group atoms (–2 × 10 CVE) fused *via* triangular faces (–2 × 48 CVE) to two tetrahedra (2 × 60 CVE) with one main group atom each (–2 × 10 CVE) is 84 CVE, and thus the cluster is two electrons deficient from the condensed polyhedra perspective ($2 \times 6(\text{Mo}) + 3 \times 9(\text{Ir}) + 4 \times 4(\text{core C}) +$

$3 \times 5(\text{Cp/Cp}^*) + 4 \times 1(\text{Ph}) + 4 \times 2(\text{CO}) = 82$ CVE). The electron deficiency of **7a** may be ameliorated by an exceptionally short Mo–Mo bond of 2.6008(7) Å *cf.* typical Mo–Mo single bond distances of 2.95–3.10 Å.^{4f–h,5}

Electrochemical and spectroelectrochemical studies

The electrochemical behavior of the new clusters was investigated using cyclic voltammetry; a representative scan (that of **8a**) is shown in Fig. 7, and details from all clusters are collected in Table 3. Under the experimental conditions, all MIR_4 clusters possess a reversible or semi-reversible first oxidation process, and an irreversible second oxidation process at *ca.* 1 V (accompanied in the case of **9a** and **9b** by a third, irreversible, oxidation process). The first oxidation processes of the phosphine-containing MIR_4 clusters are at lower potentials than those of the alkyne clusters, reflecting the strong electron-donating character of the phosphine ligands; introduction of a second phosphine, in proceeding from **5a** to **6**, results in a further 0.25 V increase in ease of oxidation. The MIR_4 clusters also exhibit reversible or semi-reversible reductions at *ca.* –1 V, with the reduction process of the alkyne-containing clusters **8a–8c** being two-electron in nature (see Fig. 7 for the cyclic voltammogram of **8a**). The M_2Ir_3 clusters exhibit two semi-reversible oxidations, together with one irreversible reduction process at large negative potentials. Across clusters **3–6**, the ease of oxidation increases on increasing the donor strength of the isocyanide (proceeding from $\text{CNC}_6\text{H}_3\text{Me}_{2-2,6}$ to CNBu^t) and replacing Mo by W, while increasing the core Ir content in proceeding to the Ir-rich clusters **5** and **6** affords the clusters with the most reversible first oxidation processes. For clusters **8** and **9**, ease of oxidation diminishes on introduction of a pendant alkyne, in proceeding from **8** to **9**, although the potential differences are small.

The reduction process of **8b** was probed at room temperature using UV-vis-NIR spectroelectrochemistry. The progressive electronic absorption of $\mathbf{8b} \rightarrow \mathbf{8b}^-$ in an optically transparent

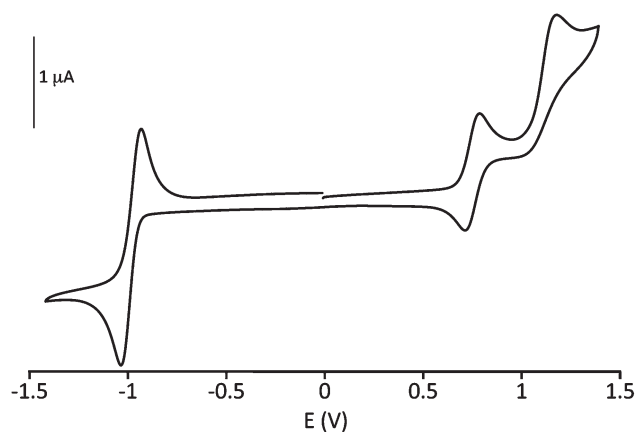


Fig. 7 Cyclic voltammogram of $\text{MoIr}_4(\mu_3\text{-}\eta^2\text{-PhC}_2\text{Ph})(\mu\text{-CO})_2(\text{CO})_6(\eta^5\text{-C}_5\text{H}_5)(\eta^5\text{-C}_5\text{Me}_5)$ (**8a**) at room temperature in CH_2Cl_2 , using the ferrocene/ferrocenium redox couple at 0.56 V as an internal standard.

Table 3 Cyclic voltammetry data of **3a–b**, **4a–d**, **5a–b**, **6**, **7a**, **8a–c**, and **9a–b**^a

	First oxidation	Second oxidation	Reduction
	$E_{1/2}$ [i_{pc}/i_{pa}]	$E_{1/2}$ (E_a) [i_{pc}/i_{pa}]	$E_{1/2}$ (E_c) [i_{pc}/i_{pa}]
$\text{Mo}_2\text{Ir}_3(\text{CNC}_6\text{H}_3\text{Me}_2\text{-}2,6)(\mu\text{-CO})_3(\text{CO})_5(\eta^5\text{-C}_5\text{H}_5)_2(\eta^5\text{-C}_5\text{Me}_5)$ (3a)	0.42 [0.5]	0.7 [0.5]	(−1.36) ^c
$\text{Mo}_2\text{Ir}_3(\text{CN}^t\text{Bu})(\mu\text{-CO})_3(\text{CO})_5(\eta^5\text{-C}_5\text{H}_5)_2(\eta^5\text{-C}_5\text{Me}_5)$ (3b)	0.34 [0.6]	0.62 [0.6]	(−1.43) ^c
$\text{Mo}_2\text{Ir}_3(\mu\text{-CO})_3(\text{CO})_5(\text{PPh}_3)(\eta^5\text{-C}_5\text{H}_5)_2(\eta^5\text{-C}_5\text{Me}_5)$ (4a)	0.44 [0.7]	0.73 [0.4]	(−1.47) ^c
$\text{W}_2\text{Ir}_3(\mu\text{-CO})_4(\text{CO})_4(\text{PPh}_3)(\eta^5\text{-C}_5\text{H}_5)_2(\eta^5\text{-C}_5\text{Me}_5)$ (4b)	0.40 [0.9]	0.65 [0.6]	(−1.52) ^c
$\text{Mo}_2\text{Ir}_3(\mu\text{-CO})_4(\text{CO})_4(\text{PPh}_3)(\eta^5\text{-C}_5\text{H}_5)_2(\eta^5\text{-C}_5\text{Me}_4\text{H})$ (4c)	0.47 [0.7]	0.73 [0.5]	(−1.40) ^c
$\text{W}_2\text{Ir}_3(\mu\text{-CO})_4(\text{CO})_4(\text{PPh}_3)(\eta^5\text{-C}_5\text{H}_5)_2(\eta^5\text{-C}_5\text{Me}_4\text{H})$ (4d)	0.43 [0.9]	0.71 [0.6]	(−1.44) ^c
$\text{MoIr}_4(\mu\text{-CO})_3(\text{CO})_6(\text{PPh}_3)(\eta^5\text{-C}_5\text{H}_5)(\eta^5\text{-C}_5\text{Me}_5)$ (5a)	0.59 [1]	(0.90) ^c	−1.14 [0.7]
$\text{WIr}_4(\mu\text{-CO})_3(\text{CO})_6(\text{PPh}_3)(\eta^5\text{-C}_5\text{H}_5)(\eta^5\text{-C}_5\text{Me}_5)$ (5b)	0.56 [0.9]	(0.86) ^c	−1.15 [1]
$\text{MoIr}_4(\mu_3\text{-CO})_2(\mu\text{-CO})_2(\text{CO})_4(\text{PPh}_3)_2(\eta^5\text{-C}_5\text{H}_5)(\eta^5\text{-C}_5\text{Me}_5)$ (6)	0.34 [1]	(0.67) ^c	−1.04 ^c
$\text{Mo}_2\text{Ir}_3(\mu_4\text{-}\eta^2\text{-PhC}_2\text{Ph})(\mu_3\text{-CPh})(\text{CO})_4(\eta^5\text{-C}_5\text{H}_5)_2(\eta^5\text{-C}_5\text{Me}_5)$ (7a)	0.51 [0.9]	0.91 [0.5]	(−1.53) ^c
$\text{MoIr}_4(\mu_3\text{-}\eta^2\text{-PhC}_2\text{Ph})(\mu_3\text{-CO})_2(\text{CO})_6(\eta^5\text{-C}_5\text{H}_5)(\eta^5\text{-C}_5\text{Me}_5)$ (8a)	0.72 [1]	(1.11) ^c	−0.99 ^b [1]
$\text{WIr}_4(\mu_3\text{-}\eta^2\text{-PhC}_2\text{Ph})(\mu_3\text{-CO})_2(\text{CO})_6(\eta^5\text{-C}_5\text{H}_5)(\eta^5\text{-C}_5\text{Me}_5)$ (8b)	0.74 [0.7]	(1.08) ^c	−1.03 ^b [1]
$\text{WIr}_4(\mu_3\text{-}\eta^2\text{-HC}_2\text{Ph})(\text{CO})_8(\eta^5\text{-C}_5\text{H}_5)(\eta^5\text{-C}_5\text{Me}_5)$ (8c) ^d	0.74 [0.7]	(1.03) ^c	−1.15 ^b [0.9]
$\text{WIr}_4(\mu_3\text{-}\eta^2\text{-PhC}_2\text{C}_6\text{H}_4(\text{C}\equiv\text{CPh})\text{-}3)(\mu_3\text{-CO})_2(\text{CO})_6(\eta^5\text{-C}_5\text{H}_5)(\eta^5\text{-C}_5\text{Me}_5)$ (9a)	0.76 [0.9]	1.08 ^c , 1.24 ^c	−0.97 [1]
$\text{WIr}_4(\mu_3\text{-}\eta^2\text{-PhC}_2\text{C}_6\text{H}_4(\text{C}\equiv\text{CPh})\text{-}4)(\mu_3\text{-CO})_2(\text{CO})_6(\eta^5\text{-C}_5\text{H}_5)(\eta^5\text{-C}_5\text{Me}_5)$ (9b)	0.77 [0.9]	1.05 ^c , 1.23 ^c	−0.95 [1]

^a CH_2Cl_2 , Ag/AgCl reference electrode, $E_{1/2}$ for FcH/FcH⁺ process at 0.56 V. ^b 2e process. ^c Irreversible process, no measurable return peak. ^d Ref. 5.

thin-layer electrochemical (OTTLE) cell is displayed in Fig. S8.† The reduction results in the disappearance of the band centered at 15 010 cm^{-1} , increases in intensity in other regions, with an isosbestic point at 16 230 cm^{-1} , and overall an increasingly featureless spectrum following reduction.

Discussion

Phosphines are the archetypical two-electron ligands, isocyanides CNR are carbonyl-like ligands with peripheral R group flexibility, and alkynes have been the cluster ligand of choice to probe C–C cleavage and formation processes relevant to Fischer–Tropsch and other catalytic transformations; as such, the phosphine, isocyanide, and alkyne chemistry of carbonyl clusters is of fundamental importance. With this in mind, the isocyanide, phosphine, and alkyne chemistry of the trigonal bipyramidal clusters **1a–1d**, **2a–2d** described above can be contrasted with that of the related lower-nuclearity tetranuclear clusters $\text{M}_2\text{Ir}_2(\text{CO})_{10}(\eta^5\text{-C}_5\text{H}_5)_2$ ($\text{M} = \text{Mo}$ **11a**, **W** **11b**) and $\text{M}\text{Ir}_3(\text{CO})_{11}(\eta^5\text{-C}_5\text{H}_5)$ ($\text{M} = \text{Mo}$ **12a**, **W** **12b**) to shed light on the impact of incorporation of the $\text{Ir}(\eta^5\text{-C}_5\text{Me}_4\text{R})$ vertex.

In the present studies, $\text{Mo}_2\text{Ir}_3(\mu\text{-CO})_3(\text{CO})_6(\eta^5\text{-C}_5\text{H}_5)_2(\eta^5\text{-C}_5\text{Me}_4\text{R})$ (**1a**, **1b**) reacted with excess isocyanide to give only mono-substitution products $\text{Mo}_2\text{Ir}_3(\mu\text{-CO})_3(\text{CO})_5(\text{CNR})(\eta^5\text{-C}_5\text{H}_5)_2(\eta^5\text{-C}_5\text{Me}_4\text{R})$ ($\text{R} = \text{Me}$, $\text{R}' = \text{C}_6\text{H}_3\text{Me}_2\text{-}2,6$ **3a**; $\text{R} = \text{Me}$, $\text{R}' = ^t\text{Bu}$ **3b**), in which core geometry, ligand disposition, and metal atom locations are maintained. In contrast, **11a** reacted with two equivalents of $\text{CNC}_6\text{H}_3\text{Me}_2\text{-}2,6$ to afford both mono- and di-substitution products, and reacted with either one or two equivalents of CNBu^t to give only the di-substituted $\text{Mo}_2\text{Ir}_2(\mu\text{-CO})_2(\text{CNBu}^t)_2(\text{CO})_6(\eta^5\text{-C}_5\text{H}_5)_2$.¹⁶ **12a** reacted with one or two equivalents of CNBu^t to afford mixtures of mono- and di- or mono- to tri-substitution products, respectively.¹⁷ In the present studies, in contrast, $\text{MoIr}_4(\mu\text{-CO})_3(\text{CO})_7(\eta^5\text{-C}_5\text{H}_5)(\eta^5\text{-C}_5\text{Me}_5)$ (**2a**) reacted with isocyanides in CH_2Cl_2 with rapid cleavage of the $\text{Ir}(\eta^5\text{-C}_5\text{Me}_5)$ vertex, evinced by the change in color from dark brown to pale yellow (in *ca.* 30 s), and the formation of $\text{MoIr}_3(\mu\text{-CO})_3(\text{CNC}_6\text{H}_3\text{Me}_2\text{-}2,6)(\text{CO})_7(\eta^5\text{-C}_5\text{H}_5)$ or $\text{MoIr}_3(\mu\text{-CO})_3(\text{CN}^t\text{Bu})(\text{CO})_7(\eta^5\text{-C}_5\text{H}_5)$; this cleavage of the $\text{Ir}(\eta^5\text{-C}_5\text{Me}_5)$ vertex occurred regardless of the stoichiometry of the isocyanide employed.

11a, **11b**, **12a**, and **12b** reacted with one equivalent of triphenylphosphine to afford mono- to di- or mono- to tri-substituted clusters, respectively.^{4a,b,6,7} In the present work, in contrast, **1a–1d** reacted with excess PPh_3 to afford mono-substituted products only and, while **2a** reacted with the same substrate to afford mono- and di-substitution products, the initial substitution is accompanied by a competitive loss of the $\text{Ir}(\eta^5\text{-C}_5\text{Me}_4\text{R})$ vertex and the formation of $\text{MoIr}_3(\mu\text{-CO})_3(\text{CO})_6(\text{PPh}_3)_2(\eta^5\text{-C}_5\text{H}_5)$. Formation of the substitution products **4a–4d** involves a core rearrangement not possible in the tetranuclear system: both group 6 metal atoms now lie in the trigonal bipyramidal clusters' equatorial planes, presumably to accommodate the bulky PPh_3 ligand which is ligated to an apical iridium atom. While the ¹H NMR spectra of the tungsten-containing clusters **4b** and **4d** are consistent with the solid-state structure (two $\eta^5\text{-C}_5\text{H}_5$ resonances), those of the molybdenum-containing clusters **4a** and **4c** have only one $\eta^5\text{-C}_5\text{H}_5$ resonance in their ¹H NMR spectra, suggestive of enhanced ligand fluxionality of the 4d metal-containing clusters.

$\text{WIr}_3(\text{CO})_{11}(\eta^5\text{-C}_5\text{H}_4\text{R})$ ($\text{R} = \text{H}$ **12b**, Me) reacted with the internal alkyne $\text{PhC}\equiv\text{CPh}$ to afford a mixture of the tetrahedral bis(alkyne) adduct $\text{WIr}_3(\mu_3\text{-}\eta^2\text{-PhC}_2\text{Ph})_2(\text{CO})_7(\eta^5\text{-C}_5\text{H}_4\text{R})$, with alkyne addition at the WIr_2 and Ir_3 faces, and the butterfly cluster $\text{WIr}_3(\mu_3\text{-CPh})\{\mu\text{-}\eta^4\text{-C}(\text{Ph})\text{C}(\text{Ph})\text{C}(\text{Ph})\}\{\mu\text{-CPh}\}(\text{CO})_5(\eta^5\text{-C}_5\text{H}_4\text{R})$ *via* alkyne C–C coupling and W–Ir and C=C cleavage, together with the (iridacyclopentadienyl)iridium complex $\text{Ir}_2\{\mu\text{-}\eta^4\text{-C}(\text{Ph})\text{C}(\text{Ph})\text{C}(\text{Ph})\text{C}(\text{Ph})\}\{\text{CO}\}_5$.¹⁸ In contrast, in the present work **2a** and **2b** reacted with alkynes by $\mu_3\text{-}\eta^2$

coordination at the non-cyclopentadienyliridium-containing Ir₃ face only.

11a and **11b** reacted in a relatively clean fashion with both internal and terminal alkynes *via* insertion into the M–M bond to give butterfly clusters M₂Ir₂(μ₄-η²-RC₂R')(μ-CO)₄(CO)₄(η⁵-C₅H₅)₂.^{4g–i,7} In contrast, **1a** reacted with the internal alkyne PhC≡CPh to give several products, one corresponding to equatorial Ir–Ir cleavage, μ₄-η²-coordination of one equivalent of alkyne, C≡C cleavage of a second equivalent of the alkyne, and coordination of μ₃-phenylmethylidyne ligands to each of the two Mo₂Ir faces, a second product presumably an isomer of the first, and a third product corresponding to a small amount of Mo₂Ir₂(μ₄-η²-PhC₂Ph)(μ-CO)₄(CO)₄(η⁵-C₅H₅)₂.

Overall, the progression from tetrahedral to trigonal bipyramidal group 6-group 9 mixed-metal cluster has resulted in species with considerable differences in reactivity: the additional Ir(η⁵-C₅Me₄R) vertex in the trigonal bipyramidal clusters is prone to cleavage, being removed to varying extents in reactions with isocyanides, phosphines or alkynes. Isocyanides and phosphines react rapidly with the tetrahedral clusters to afford mixtures of products with varying levels of substitution, while the trigonal bipyramidal clusters favor mono-substitution, the sole example of a di-substituted cluster being formed under comparatively forcing conditions. The C–C bond formation between two alkyne units that forms η³-C(Ph)C(Ph)C(Ph) and η⁴-C(Ph)C(Ph)C(Ph)C(Ph) ligands on the tetrahedral clusters has not thus far been observed with the trigonal bipyramidal clusters and, for the latter, only one low-yielding example of C≡C cleavage has been conclusively established (**7a**). Examples of μ₄-η²-PhC₂Ph ligands have been identified with both the tetrahedral and trigonal bipyramidal clusters; in the former case [Mo₂Ir₂(μ₄-η²-PhC₂Ph)(μ-CO)₄(CO)₄(η⁵-C₅H₅)₂], the C₂ vector is parallel to an intact Ir–Ir linkage, forming a pseudo-octahedral Mo₂Ir₂C₂ core, while in the latter case (**7a**), the C₂ vector is perpendicular to a cleaved Ir–Ir linkage, the Mo₂Ir₃C₂ forming a distorted pentagonal bipyramid.

A fundamental interest in progression from homometallic to heterometallic clusters is the anticipation that introduction of the heterometal(s) should enhance or modify reactivity. The present system permits examination of this possibility *via* a contrast of homometallic iridium clusters with isostructural mixed group 6-iridium clusters. Phosphine substitution at Ir₄(CO)₁₂ under thermal conditions necessitates temperatures of *ca.* 110 °C and affords tri- or tetra-substitution products.¹⁹ In contrast, as mentioned above, phosphine substitution at **11a**, **11b** and **12a**, **12b** proceeds stoichiometrically at room temperature with one or two equivalents (one to three for the latter) to afford mono- and di-substitution products (mono- to tri-substitution for the latter) in excellent yields.^{4a,b,6,7} Examples of isocyanide substitution at Ir₄(CO)₁₂ are sparse,^{20,21} and require forcing conditions; reactions with CNBu^t proceed in refluxing chlorobenzene to afford mono- and di-substituted products in low yields.^{22,23} In contrast, **11a**, **11b**, **12a**, and **12b** react at room temperature to afford mono- or di-substitution products in excellent yields.^{16,24} The lack of

solubility of Ir₄(CO)₁₂, which retards direct phosphine and isocyanide substitution, also impedes its reactivity towards alkynes; this is restricted to the activated alkyne MeO₂CC≡CCO₂Me (necessitating irradiation) and phosphinoalkynes that react *via* initial *P*-coordination.²⁵ In contrast, **11a**, **11b**, **12a**, and **12b** react with a broad range of alkynes between room temperature and refluxing toluene (milder conditions for **11a**, **11b**, and for M = Mo) to afford a diverse range of products incorporating one to three alkyne residues.^{4c,g–k,7,17,26} Thus, the incorporation of the heterometal(s) result(s) in significantly enhanced reactivity at tetranuclear core nuclearity.

The contrast is also stark with pentanuclear clusters. The few extant pentairidium clusters²⁷ possess square pyramidal^{27a,b} or trigonal bipyramidal^{27c–e} cores, with all except trigonal bipyramidal [Ir₅(μ-H)(μ-CO)₂(CO)₁₀][–] being derived from a *P*-ligated lower nuclearity precursor. [Ir₅(μ-H)(μ-CO)₂(CO)₁₀]^{2–} has limited stability and requires careful handling, necessitating the use of large cations, and is converted into tetrahedral [Ir₄(μ-H)(μ-CO)₃(CO)₈][–] in the presence of CO and into [Ir₆(μ-CO)₃(CO)₁₂]^{2–} when reacted with mild oxidants such as AuCl(PPh₃).^{27c} In contrast, the trigonal bipyramidal clusters **1a–1d**, **2a** and **2b** are stable and easy to handle. Indeed, the present studies have shown that increasing group 6 metal content enhances core stability towards donor ligands isocyanides and phosphines; ligated-iridium vertex removal diminishes on proceeding from pentairidium to molybdenum/tungsten-tetrairidium and then dimolybdenum/ditungsten-triiridium clusters.

The only phosphine-ligated pentairidium clusters Ir₅(μ-*P,C*-PPh₂C₆H₄-2)(μ-CO)₄(CO)₇(PPh₃) and Ir₅(μ-CO)₃(Ph)(CO)₉(PPh₃) both bear apical iridium-coordinated phosphine ligands,^{27d} similar to **4a–4d** and **5a**, **5b** in the present study. Reaction of Ir₅(μ-CO)₃(Ph)(CO)₉(PPh₃) with PPh₃ necessitated refluxing benzene and afforded Ir₅(μ-*P,C*-PPh₂C₆H₄-2)(μ-CO)₄(CO)₇(PPh₃) following orthometallation of a phosphine phenyl ring and loss of benzene.^{27d} Both phosphorus atoms in the latter cluster are found at apical iridium sites, in contrast to **6** for which apical, equatorial ligation is seen due to pentamethylcyclopentadienyl ligation of one of the apical iridium atoms.

There is no extant pentairidium isocyanide or alkyne chemistry.²⁸ *C*-ligands have been introduced into pentairidium clusters *via* reaction of the cyclooctadiene (COD)-ligated {Ir(μ-Cl)-(η⁴-1,2,5,6-C₈H₁₂)₂} with a tetrairidium precursor at 80 °C,^{27e} the resultant species bearing one or two apical iridium-coordinated COD ligands. Thermolysis at 98 °C resulted in Ir–Ir bond cleavage and a change in core nuclearity. In contrast, alkyne addition with the mixed group 6-iridium clusters proceeded with no change in core nuclearity and, in the case of the molybdenum/tungsten-tetrairidium clusters, reaction under very mild conditions to afford alkyne adducts.

Electrochemical studies of **1a–1d**, **2a** and **2b** revealed both oxidation and reduction is accessible (with respect to the resting state), the oxidation processes being the more reversible, and increasingly so on decreasing Ir content of the clusters, replacing W by Mo, and increasing alkylation of the cyclopentadienyl ligands.⁵ There is no report of the electroche-

mical behavior of $[\text{Ir}_5(\mu\text{-H})(\mu\text{-CO})_2(\text{CO})_{10}]^{2-}$, but its aforementioned oxidative sensitivity^{27c} is consistent with this trend. Introduction of isocyanide, phosphine or alkyne residue in proceeding to the current ligand-substituted series results in an increased ease of oxidation and increased difficulty in reduction (although many of the latter processes are irreversible, so comment must be cautious). Incorporation of these ligands therefore serves to tune the electron richness at the cluster. Finally, the reductive spectroelectrochemical study of **8b** complements the oxidative spectroelectrochemical studies of **1a** and **2a** in our previous report,⁵ the former cluster being the molybdenum-containing homologue of the tungsten-containing precursor to **8b**. Oxidation of $\text{MoIr}_4(\mu\text{-CO})_3(\text{CO})_7(\eta^5\text{-C}_5\text{H}_5)(\eta^5\text{-C}_5\text{Me}_5)$ resulted in a UV-vis-NIR spectrum similarly featureless to that observed following reduction of **8b**; thus, spectral features become increasingly indistinct with both oxidation and reduction in this system.

Conclusions

The studies described herein have demonstrated facile functionalization of pentanuclear molybdenum/tungsten-iridium clusters and thereby access to a range of systematically-derivatized species not currently accessible in the homometallic pentairidium system. The ligand substitution studies have shown that cluster core stability and ease of derivatization is diminished on proceeding from tetranuclear to pentanuclear clusters, but is enhanced on increasing the group 6 metal content, and have thereby demonstrated the benefit in proceeding from homometallic to heterometallic environment. Ligand substitution generally proceeds at sites that can be rationalized on steric grounds (non-cyclopentadienyl-ligated iridium vertices, and initial substitution at an apical site if triphenylphosphine and an equatorial site if isocyanide). As judged by the potential of the first oxidation processes accessed from the cluster resting states, the electron richness of the present series of ligand-substituted clusters is tuned in a rational fashion.

The current studies have also highlighted significant differences in alkyne reactivity between tetranuclear group 6-iridium clusters and the pentanuclear analogues, but also illustrate the desirable metallo-, bond-, and face-selectivity for reactions at mixed-metal clusters; in addition to the aforementioned iridium-specific ligand substitution, clusters $\text{M}_2\text{Ir}_2(\mu_4\text{-}\eta^2\text{-RC}_2\text{R}')(\mu\text{-CO})_4(\text{CO})_4(\eta^5\text{-C}_5\text{H}_5)_2$ form in high yield by bond-specific insertion of an alkyne into the M–M linkage of the precursor (with M–Ir and Ir–Ir, one of three distinct core bond types), while clusters $\text{M}\text{Ir}_4(\mu_3\text{-}\eta^2\text{-PhC}_2\text{R})(\mu_3\text{-CO})_2(\text{CO})_6(\eta^5\text{-C}_5\text{H}_5)(\eta^5\text{-C}_5\text{Me}_5)$ (**8**, **9**) form in good yield by face-specific addition at Ir_3 (with MIr_2 , one of two distinct core face types).

Related articles

Mixed-Metal Cluster Chemistry. Part 34. Part 33: M. D. Randles, P. V. Simpson, V. Gupta, J. Fu, G. J. Moxey,

T. Schwich, A. L. Criddle, S. Petrie, J. G. MacLellan, S. R. Batten, R. Stranger, M. P. Cifuentes, M. G. Humphrey, *Inorg. Chem.*, 2013, **52**, 11256.

Abbreviations

Cp	($\eta^5\text{-C}_5\text{H}_5$)
Cp*	($\eta^5\text{-C}_5\text{Me}_5$)
Cp [#]	($\eta^5\text{-C}_5\text{Me}_4\text{H}$)
TLC	Thin-layer chromatography

Acknowledgements

We thank the Australian Research Council (ARC) for financial support. M.D.R. was the recipient of an Australian Postgraduate Award, J.F. is the recipient of a China Scholarship Council ANU Postgraduate Scholarship, M.P.C. thanks the ARC for an Australian Research Fellowship, and M.G.H. held an ARC Australian Professorial Fellowship.

Notes and references

- (a) *The Chemistry of Metal Cluster Complexes*, ed. D. F. Shriver, H. D. Kaesz and R. D. Adams, VCH, New York, 1990; (b) *Physics and Chemistry of Metal Cluster Complexes*, ed. L. L. de Jongh, Kluwer, Amsterdam, 1994; (c) P. Braunstein, L. A. Oro and P. R. Raithby, *Metal Clusters in Chemistry*, Wiley-VCH, Weinheim, Germany, 1999.
- (a) R. D. Adams and F. A. Cotton, *Catalysis by Di- and Polynuclear Metal Cluster Complexes*, Wiley-VCH, New York, 1998. Higher-nuclearity clusters continue to attract interest. See, for example: (b) E. G. Mednikov, M. C. Jewell and L. F. Dahl, *J. Am. Chem. Soc.*, 2007, **129**, 11619; (c) E. G. Mednikov and L. F. Dahl, *J. Am. Chem. Soc.*, 2008, **130**, 14813; (d) C. Femoni, M. C. Iapalucci, G. Longoni, J. Wolowska, S. Zacchini, P. Zanello, S. Fedi, M. Ricco, D. Ponticoli and M. Mazzani, *J. Am. Chem. Soc.*, 2010, **132**, 2919; (e) D. S. Dolzhenkov, M. C. Iapalucci, G. Longoni, C. Tiozzo, S. Zacchini and C. Femoni, *Inorg. Chem.*, 2012, **51**, 11214.
- (a) M. C. Comstock and J. R. Shapley, *Coord. Chem. Rev.*, 1995, **143**, 501; (b) S. M. Waterman, N. T. Lucas and M. G. Humphrey, *Adv. Organomet. Chem.*, 2000, **46**, 47.
- See, for example: (a) J. Lee, M. G. Humphrey, D. C. R. Hockless, B. W. Skelton and A. H. White, *Organometallics*, 1993, **12**, 3468; (b) S. M. Waterman, M. G. Humphrey, V.-A. Tolhurst, D. C. R. Hockless, B. W. Skelton and A. H. White, *Organometallics*, 1996, **15**, 934; (c) S. M. Waterman, M. G. Humphrey, V.-A. Tolhurst, M. I. Bruce, P. J. Low and D. C. R. Hockless, *Organometallics*, 1998, **17**, 5789; (d) S. M. Waterman and M. G. Humphrey, *Organometallics*, 1999, **18**, 3116; (e) S. M. Waterman, J. Lee, M. G. Humphrey, G. E. Ball and D. C. R. Hockless, *Organometallics*, 1999, **18**, 2440; (f) N. T. Lucas, J. P. Blitz, S. Petrie, R. Stranger,

- M. G. Humphrey, G. A. Heath and V. Otieno-Alego, *J. Am. Chem. Soc.*, 2002, **124**, 5139; (g) N. T. Lucas, E. G. A. Notaras, M. P. Cifuentes and M. G. Humphrey, *Organometallics*, 2003, **22**, 284; (h) N. T. Lucas, E. G. A. Notaras, S. Petrie, R. Stranger and M. G. Humphrey, *Organometallics*, 2003, **22**, 708; (i) E. G. A. Notaras, N. T. Lucas, M. G. Humphrey, A. C. Willis and A. D. Rae, *Organometallics*, 2003, **22**, 3659; (j) G. T. Dalton, L. Viau, S. M. Waterman, M. G. Humphrey, M. I. Bruce, P. J. Low, R. L. Roberts, A. C. Willis, G. A. Koutsantonis, B. W. Skelton and A. H. White, *Inorg. Chem.*, 2005, **44**, 3261; (k) M. D. Randles, R. D. Dewhurst, M. P. Cifuentes and M. G. Humphrey, *Organometallics*, 2012, **31**, 2582.
- 5 M. D. Randles, P. V. Simpson, V. Gupta, J. Fu, G. J. Moxey, T. Schwich, A. L. Criddle, S. Petrie, J. G. MacLellan, S. R. Batten, R. Stranger, M. P. Cifuentes and M. G. Humphrey, *Inorg. Chem.*, 2013, **52**, 11256.
- 6 N. T. Lucas, I. R. Whittall, M. G. Humphrey, D. C. R. Hockless, M. P. S. Perera and M. L. Williams, *J. Organomet. Chem.*, 1997, **540**, 147.
- 7 N. T. Lucas, M. G. Humphrey, P. C. Healy and M. L. Williams, *J. Organomet. Chem.*, 1997, **545–546**, 519.
- 8 Z. Otwinowski and W. Minor, *Methods Enzymol.*, 1997, **276**, 307.
- 9 R. H. Blessing, *Acta Crystallogr., Sect. A: Fundam. Crystallogr.*, 1995, **51**, 33.
- 10 P. W. Betteridge, J. R. Carruthers, R. I. Cooper, K. Prout and D. J. Watkin, *J. Appl. Crystallogr.*, 2003, **36**, 1487.
- 11 G. M. Sheldrick, *Acta Crystallogr., Sect. A: Fundam. Crystallogr.*, 2008, **64**, 112.
- 12 O. V. Dolomanov, L. J. Bourhis, R. J. Gildea, J. A. K. Howard and H. Puschmann, *J. Appl. Crystallogr.*, 2009, **42**, 339.
- 13 P. v. d. Sluis and A. L. Spek, *Acta Crystallogr., Sect. A: Fundam. Crystallogr.*, 1990, **46**, 194.
- 14 H. D. Flack, *Acta Crystallogr., Sect. A: Fundam. Crystallogr.*, 1983, **39**, 876.
- 15 A. L. Spek, *Acta Crystallogr., Sect. D: Biol. Crystallogr.*, 2009, **65**, 148.
- 16 A. J. Usher, M. G. Humphrey and A. C. Willis, *J. Organomet. Chem.*, 2003, **678**, 72.
- 17 A. J. Usher, M. G. Humphrey and A. C. Willis, *J. Organomet. Chem.*, 2003, **682**, 41.
- 18 (a) J. R. Shapley, C. H. McAteer, M. R. Churchill and L. V. Biondi, *Organometallics*, 1984, **3**, 1595; (b) E. G. A. Notaras, N. T. Lucas, J. P. Blitz and M. G. Humphrey, *J. Organomet. Chem.*, 2001, **631**, 143.
- 19 (a) R. Whyman, *J. Organomet. Chem.*, 1970, **24**, C35; (b) R. Whyman, *J. Organomet. Chem.*, 1971, **29**, C36; (c) A. J. Drakesmith and R. Whyman, *J. Chem. Soc., Dalton Trans.*, 1973, 362; (d) P. E. Cattermole, K. G. Orell and A. G. Osborne, *J. Chem. Soc., Dalton Trans.*, 1974, 328; (e) K. J. Karel and J. R. Norton, *J. Am. Chem. Soc.*, 1974, **96**, 6812.
- 20 Isocyanide derivatives of (non-carbonyl) tetrairidium pyrazolato^{20a} and sulfido^{20b} clusters have been reported: (a) C. Tejel, M. A. Ciriano, J. A. Lopez, F. J. Lahoz and L. A. Oro, *Angew. Chem., Int. Ed.*, 1998, **37**, 1542; (b) H. Seino, A. Saito, H. Kajitani and Y. Mizobe, *Organometallics*, 2008, **27**, 1275.
- 21 Isocyanide substitution at fullerene-ligated tetrairidium clusters has been demonstrated: (a) G. Lee, Y.-J. Cho, B. K. Park, K. Lee and J. T. Park, *J. Am. Chem. Soc.*, 2003, **125**, 13920; (b) B. K. Park, G. Lee, K. H. Kim, H. Lee, C. Y. Kang, M. A. Miah, J. Jung, Y.-K. Han and J. T. Park, *J. Am. Chem. Soc.*, 2006, **128**, 11160.
- 22 G. F. Stuntz and J. R. Shapley, *J. Organomet. Chem.*, 1981, **213**, 389.
- 23 The difficulty in effecting simple thermal substitution resulted in its replacement by more effective alternatives. (i) Trimethylamine-*N*-oxide promoted substitution: (a) J. R. Shapley, G. F. Stuntz, M. R. Churchill and J. P. Hutchinson, *J. Chem. Soc., Chem. Commun.*, 1979, 219; (b) Ref. 22 (ii) Reaction at [Ir₄(I)(CO)₁₁]⁻: (c) A. Orlandi, R. Ros and R. Roulet, *Helv. Chim. Acta*, 1991, **74**, 1464.
- 24 S. M. Waterman, M. G. Humphrey and D. C. R. Hockless, *J. Organomet. Chem.*, 1999, **579**, 75.
- 25 (a) P. F. Heveldt, B. F. G. Johnson, J. Lewis, P. R. Raithby and G. M. Sheldrick, *J. Chem. Soc., Chem. Commun.*, 1978, 340; (b) C. Barnes, in *Comprehensive Organometallic Chemistry II*, ed. E. W. Abel, F. G. A. Stone and G. Wilkinson, Pergamon Press, Oxford, U.K., 1995, vol. 8, ch. 4.
- 26 (a) G. T. Dalton, A. C. Willis and M. G. Humphrey, *J. Cluster Sci.*, 2004, **15**, 291; (b) M. D. Randles, N. T. Lucas, M. P. Cifuentes, M. G. Humphrey, M. K. Smith, A. C. Willis and M. Samoc, *Macromolecules*, 2007, **40**, 7807.
- 27 (a) D. Braga and M. D. Vargas, *J. Chem. Soc., Chem. Commun.*, 1988, 1443; (b) R. Khattar, S. Naylor, M. D. Vargas, D. Braga and F. Grepioni, *Organometallics*, 1990, **9**, 645; (c) R. Della Pergola, L. Garlaschelli, M. Manassero, M. Sansoni and D. Strumolo, *J. Cluster Sci.*, 2001, **12**, 23; (d) R. D. Adams and M. Chen, *Organometallics*, 2011, **30**, 5867; (e) R. D. Adams and M. Chen, *Organometallics*, 2012, **31**, 445.
- 28 Reactions of hexairidium clusters with alkynes have been reported, reflecting the increased stability of the octahedral core: A. Ceriotti, R. Della Pergola, F. Demartin, L. Garlaschelli, M. Manassero and N. Masciocchi, *Organometallics*, 1992, **11**, 756.

Copyright of Dalton Transactions: An International Journal of Inorganic Chemistry is the property of Royal Society of Chemistry and its content may not be copied or emailed to multiple sites or posted to a listserv without the copyright holder's express written permission. However, users may print, download, or email articles for individual use.